Condensation of a nuclear mRNA export factor regulates mRNA transport during stress

Stephanie Heinrich[1,#], Maria Hondele[1,2], Désirée Marchand[1], Carina Patrizia Derrer[1], Mostafa Zedan[1], Alexandra Oswald[1], Federico Uliana[1], Roberta Mancini[1], David Grunwald[3], Karsten Weis[1,#]

[1] Institute of Biochemistry, ETH Zurich, Otto-Stern-Weg 3, 8093 Zurich, Switzerland
[2] Biozentrum, University of Basel, Klingelbergstrasse 50/70, 4056 Basel, Switzerland
[3] University of Massachusetts Medical School, RNA Therapeutics Institute, 368 Plantation Street, Worcester MA 01605, USA
[#] Corresponding author, lead contact: karsten.weis@bc.biol.ethz.ch

Highlights

- The nuclear Poly(A)-binding protein Nab2 forms condensates upon acute cellular depletion of the DEAD-box ATPase Dbp5
- Nab2 dimerization but not its intrinsically disordered regions (IDRs) are essential for condensation *in vitro* and *in vivo*
- Glucose stress leads to global mRNA retention in the nucleus and depends on Nab2 condensation
- Nab2 condensation confers selectivity of RNA retention during glucose stress
- Proper Nab2 condensation is essential for survival after prolonged stress

Summary

Unidirectional mRNA transport from the nucleus to the cytoplasm via nuclear pore complexes is an essential step in eukaryotic gene expression. Although factors involved in mRNA transport have been characterized, a comprehensive mechanistic understanding of this critical process and its regulation is lacking. Here, we use single RNA imaging to show that cells use selective mRNA retention to re-wire mRNA export during stress. We demonstrate that upon glucose withdrawal the essential export factor Nab2 forms RNA-dependent condensates in the nucleus blocking bulk mRNA export while selectively allowing the transport of stress-induced mRNAs. This is accompanied by reduced abundance of the DEAD-box ATPase Dbp5 at the nuclear pore, and experimental Dbp5 depletion triggers Nab2 condensation and nuclear mRNA accumulation. Condensation can be recapitulated *in vitro*, with Nab2 forming RNA-dependent liquid droplets, which fail to form in the presence of active Dbp5. Our results suggest that cells use condensation to selectively regulate mRNA export and to control gene expression during stress.

Keywords

RNA, mRNA export, phase separation, condensation, Nab2, DEAD-box ATPase Dbp5, glucose stress

Introduction

Gene expression in eukaryotic cells is intricately regulated and aided by subcellular compartmentalization. The nuclear envelope serves as a physical barrier and separates nuclear transcription from cytoplasmic translation processes. Embedded in the nuclear membrane are nuclear pore complexes (NPC) that regulate the passage of macromolecules into and out of the nucleus, including the export of messenger RNAs (mRNA) that relay the genetic information to the protein translation machinery in the cytoplasm (reviewed in (Ashkenazy-Titelman et al., 2020; De Magistris, 2021)). mRNAs are extensively processed in the nucleus and undergo a coordinated series of modifications before export, which includes the addition of a 5' m7G cap structure, removal of introns through splicing, and 3' end processing for poly(A) tail synthesis (reviewed in (Herzel et al., 2017; Rambout and Maquat, 2020; Shi and Manley, 2015)). To facilitate these processes, a range of RNA-binding proteins (RBPs) form a dynamic mRNA coat on the nascent mRNA, either co-transcriptionally or post-transcriptionally in the nucleoplasm. The orderly assembly of this coat is essential for forming an export-competent mRNA-protein (mRNP) particle (reviewed in (Ashkenazy-Titelman et al., 2020; Singh et al., 2015)). Early binding proteins include the cap-binding complex (CBC; comprising Cbc1 (CBP80 in vertebrates) and Cbc2 (CBP20)), which binds co-transcriptionally to the 5'-cap of nascent mRNAs (Izaurralde et al., 1994). Another early binding complex, the transcription and export (TREX) complex (consisting of the multi-subunit THO subcomplex, the DEAD-box ATPase Sub2 (UAP56), and the RNA binding protein Yra1 (ALYREF)) connects 3' end processing with mRNA export (Katahira, 2012; Pühringer et al., 2020; Sträßer et al., 2002; Sträßer and Hurt, 2001). Similar to TREX, the abundant class of serine-arginine-rich (SR) proteins (e.g., yeast Npl3) has been implicated in a multitude of mRNA processing steps, such as co-transcriptional splicing, 3' end processing and nuclear export (reviewed in (Wegener and Müller-McNicoll, 2019)). The export factor Nab2 (ZC3H14) is recruited to the poly(A) tail of the pre-mRNA and is involved in nuclear mRNA surveillance protecting mRNAs against degradation by the nuclear exosome (Anderson et al., 1993; Hector et al., 2002; Schmid et al., 2012, 2015). Nab2 has been shown to dimerize on RNA and to play a role in proper 3' end processing of nascent transcripts to terminate polyadenylation and facilitate compaction of the mRNP (Aibara et al., 2017; Alpert et al., 2020; Fasken et al., 2019). In addition, it directly interacts with the NPC component Mlp1 (Green et al., 2003). The translocation of mature transcripts through NPCs is mediated by the export factor Mex67:Mtr2 (NXF1:NXT1), which functions akin to a mobile nuclear pore protein facilitating transport by binding to both mRNPs as well as phenylalanine–glycine (FG)-containing NPC components (nucleoporins)(Ashkenazy-Titelman et al., 2020; Derrer et al., 2019). On the cytoplasmic face of the NPC, the essential DEAD-box ATPase Dbp5 (DDX19B), aided by its interaction partners Nup159 (NUP214), Gle1 and inositol hexakisphosphate (IP_6), has been suggested to remodel emerging mRNPs by removing export factors such as Nab2 from the mRNA, thereby facilitating their release into the cytoplasm (Alcázar-Román et al., 2006; Tran et al., 2007; Weirich et al., 2006). However, these models are mainly based on *in vitro* studies (Montpetit et al., 2011; Noble et al., 2011; Tran et al., 2007), and the *in vivo* function of Dbp5 in directional transport remains unclear.

In addition to membrane-based compartmentalization, cells also organize their content in membraneless organelles through liquid-liquid phase separation (LLPS)(reviewed in (Banani et al., 2017; Shin and Brangwynne, 2017). Formation of these biomolecular condensates depends on weak, multivalent interactions and proteins undergoing LLPS often contain low-complexity domains with intrinsically disordered regions (IDRs). IDRs are frequently found in RNA-binding proteins and RNA can enhance their propensity to form condensates (reviewed in (Roden and Gladfelter, 2021)). LLPS is an evolutionarily ancient and conserved self-organizing principle (Hondele et al., 2019; Riback et al., 2017). Within a cell,

many structures can be defined as membraneless organelles and they have been implicated in various aspects of gene expression regulation (reviewed in (Banani et al., 2017)). For example, stress conditions such as nutrient depletion or acute temperature shifts have been shown to induce the formation of cytoplasmic condensates such as P-bodies (PB) or stress granules (SG) (Kroschwald et al., 2015; Sheth and Parker, 2003). If LLPS plays a role in mRNA export is unknown.

Here, we report that nuclear condensation of the mRNA export factor Nab2 selectively regulates mRNA transport in glucose stress, and that this process is modulated by the activity of the DEAD-box ATPase Dbp5. Nab2 condensation leads to the retention of bulk mRNAs in the nucleus but allows selective export of stress-induced transcripts, which is impaired in Nab2 mutants that affect the state of the condensate. Our results establish condensation as a regulator of mRNA transport during cellular stress and provide mechanistic insights into mRNA export regulation.

Results

Acute Dbp5 depletion causes nuclear mRNA accumulation and Nab2 mobility reduction

To characterize the function of Dbp5 in directional mRNA export *in vivo*, we employed the auxin-inducible acute protein depletion system in the budding yeast *Saccharomyces cerevisiae* (Nishimura 2009, Fig. 1A, 'degron'). Addition of auxin led to the efficient and specific depletion of Dbp5 with a half-time of approx. 12 min (Fig. S1A,B), without affecting the overall NPC composition based on the quantification of selected nucleoporins using a previously established method (NuRIM (Rajoo et al., 2018); Fig. S1C). Dbp5 depletion did not affect protein export as an NLS-NES-2xGFP reporter did not enrich in the nucleus after auxin addition. In contrast, blocking Xpo1-dependent export using Leptomycin B (LMB) in an LMB-sensitive Xpo1 mutant (Neville and Rosbash, 1999) strongly impaired nuclear export of the GFP reporter (Fig. S1D-G). Furthermore, addition of LMB to cells that were already Dbp5-depleted shifted the GFP reporter distribution towards the nucleus. This shows that nuclear protein import and export remain functional when Dbp5 is depleted (Fig. S1D-G).

Upon Dbp5 depletion, we observed a global nuclear retention of poly(A) RNA using fluorescence *in situ* hybridization (FISH) with an oligo(dT)30 probe, similar to previous reports using temperature-sensitive *dbp5* alleles (Fig. S1H)(Hodge et al., 1999; Snay-Hodge et al., 1998). To investigate whether this oligo(dT)30 staining corresponds to the nuclear retention of mRNA, we examined the export of individual mRNAs. To this end, we marked transcripts of an essential gene, glutamine-fructose-6-phosphate amidotransferase (*GFA1)*, with the PP7-PCP stem loop labeling system ((Larson et al., 2011), Fig. 1A) in the Dbp5 degron background. In the presence of Dbp5, the GFA1-PP7 transcripts were mostly localized in the cytoplasm (Fig. 1B). Upon Dbp5 depletion, transcripts accumulated in the nucleus close to the nuclear periphery. Interestingly, the mobility of nuclear mRNAs was reduced in the absence of Dbp5 based on single particle tracking results obtained from a custom-built microscope ((Smith et al., 2015), Fig. 1C, Video S1, Video S2). To test whether the dynamics of nuclear export factors were also affected, we performed fluorescence recovery after photobleaching (FRAP) measurements after Dbp5 depletion. The nuclear dynamics of the export factors Yra1 and Npl3 as well as an NLS-GFP(3x) control did not change when Dbp5 was depleted (Fig. S2A-F). However, the nuclear mobility of the poly(A)-binding protein Nab2 was dramatically reduced (Fig. 1D-F), with a >5-fold reduction of recovery half-time in the absence of Dbp5. Intriguingly, FRAP of approximately half of the nucleus showed very slow recovery of Nab2 in the entire bleached region (Fig. 1F). The reduction in Nab2 mobility is RNA-dependent as additional depletion of a polymerase II subunit (Rpb2-AID) reverted the phenotype (Fig.

1G,H) by reducing the amount of poly(A) RNA in the nucleus (Fig. S2G). The mRNA-dependent mobility of Nab2 in the nucleus controlled by the DEAD-box ATPase Dbp5 is reminiscent of PBs or SGs which are mRNA-dependent cytoplasmic condensates regulated by the DEAD box ATPases, Dhh1 and Ded1, respectively (Hilliker et al., 2011; Hondele et al., 2019; Mugler et al., 2016; Teixeira and Parker, 2007). Our results therefore suggest that Nab2 forms an mRNA-dependent condensate in the nucleus *in vivo*, whose dynamics depend on the presence of Dbp5.

Nab2 phase-separates *in vitro*, which is reverted by active Dbp5

The sequence of Nab2 shows many hallmarks of RNA-binding proteins that can undergo LLPS. In addition to an N-terminal domain required for Mlp1 binding and mRNA export, Nab2 contains a Q-rich domain of unknown function (QQQP), an RGG domain with an internal nuclear localization signal (NLS), and 7 zinc fingers (ZnF), of which ZnF5-7 are essential for RNA binding (Fig. S2H)(Anderson et al., 1993; Marfatia et al., 2003; Soniat et al., 2013). Furthermore, according to PONDR, a predictor of naturally disordered regions (Li et al., 1999; Romero et al., 1997), the Q-rich domain and the RGG domain are intrinsically disordered (Fig. S2H). We therefore wanted to examine whether Nab2 can undergo phase separation *in vitro*. Intriguingly, in the presence of poly(A) RNA recombinant Nab2 formed liquid droplets at close to endogenous concentrations (Fig. 2A and S2I,J). These droplets were dynamic as they had the ability to fuse and grow over time (Video S3), and were mildly sensitive to the aliphatic alcohol 1,6-hexanediol, consistent with them being formed via liquid-liquid phase separation (Fig. S2K,L).

Nab2 condensates form at physiological salt concentrations and are pH-dependent (Fig. 2B). In addition to poly(A), Nab2 can form condensates with other single-nucleoside polymers (poly(U)/poly(G)/poly(C), Fig. 2C), suggesting that Nab2 does not exclusively bind to the poly(A) tail of mRNAs. Indeed, previous reports have shown that Nab2 can bind also non-poly(A) RNA *in vitro* (Anderson et al., 1993) and associates with mRNA regions upstream of the poly(A) tail *in vivo* (Tuck and Tollervey, 2013).

We next wanted to understand the interplay between Nab2 and Dbp5. *In vitro* work by Tran *et al.* demonstrated that Dbp5 is able to replace Nab2 from poly(A) RNA (Tran et al., 2007). Strikingly, co-incubation of Nab2 with wild type Dbp5 and its ATPase-activators Gle1 and IP_6 (Alcázar-Román et al., 2006; Weirich et al., 2006) prevented condensate formation (Fig. S2M). This was dependent on Dbp5 as Gle1 and IP_6 alone did not block droplet formation (Fig. S2M). Furthermore, a dominant-active Dbp5 mutant, $Dbp5^{\Delta N90}$, which functions independently of Gle1 and IP_6 (Montpetit et al., 2011), also inhibited Nab2 condensation (Fig. 2D). Conversely, the ATP-locked form of Dbp5, $Dbp5^{\Delta N90\text{-}DQAD}$, was unable to affect Nab2 condensation (Fig. 2D), suggesting that the ATP hydrolysis cycle is required to inhibit Nab2 condensation.

Together, our results indicate that RNA-dependent Nab2 condensation can be regulated by the ATPase activity of Dbp5 and that loss of Dbp5 activity triggers Nab2 condensation.

Glucose stress causes reduction of nuclear Nab2 dynamics and bulk nuclear mRNA retention

Having established that Nab2 forms a condensate *in vitro*, we next asked if Nab2 condensation can also be observed in physiologically relevant conditions in cells. It has been previously observed that Dbp5 re-localizes from the NPC to the nucleoplasm in specific stress conditions, such as acute ethanol stress (Izawa et al., 2005; Takemura et al., 2004). We therefore tested Dbp5 localization upon nutrients stress. Interestingly, NPC localization of Dbp5, but not its cytoplasmic NPC-interaction partners Nup159 and Gle1, is reduced both upon acute (30 min –DEX) and prolonged (24 hrs –DEX) glucose starvation. (Fig. 3A,B and S3A,B). Furthermore, in these starvation conditions, export of bulk mRNA is blocked (Fig.

3C,D). Intriguingly, glucose starvation resulted in the formation of predominantly nuclear Nab2 foci, while other export factors such as Yra1 and Npl3 were unaffected (Fig. 3C,D and S3C,D). Discrete Nab2 foci formed during short-term glucose withdrawal and focus formation was enhanced upon long-term glucose starvation (Fig. 3C,D). Nab2 foci were mostly resistant to 1,6-hexanediol treatment, which dissolves cytoplasmic membraneless organelles such as P-bodies, but not stress granules (Fig. S4A-C) (Kroschwald et al., 2015). Nab2 focus formation was accompanied by nuclear accumulation of poly(A) RNA in a punctate pattern overlapping with Nab2 foci (Fig. 3C, D). The poly(A) RNA that was retained in these foci seemed to correspond to intact transcripts as they also showed co-localization with the cap-binding complex proteins Cbc1 and Cbc2 ((Izaurralde et al., 1994), Fig. S4G). Nab2-mRNA foci were reversible, as release from starvation conditions into medium containing glucose led to the full dispersal of Nab2 in the nucleus within an hour (Fig. S4D). These results suggest that Nab2 condensation confers nuclear enrichment of bulk mRNA in long-term starvation.

We then tested Nab2 mobility in short-term and long-term starvation. Similar to acute Dbp5 depletion, we observed a reduction in nuclear dynamics after 30 min of acute glucose starvation (Fig. 3E,F). This phenotype was even more prominent upon long-term glucose starvation (24 hrs) (Fig. 3G,H). The reduction in dynamics was specific for Nab2 as the mobility of other export factors such as Npl3 and Yra1 was not affected (Fig. S3E-H). Nab2 mobility reduction was dependent on the presence of mRNA and treatment with the transcription inhibitor thiolutin (Tipper, 1973) restored Nab2 mobility to the levels of non-stressed cells (Fig. S4E,F). We next wanted to examine whether Nab2 focus formation is triggered by the loss of Dbp5 from the NPC during long-term stress. Intriguingly, when Dbp5 was prevented from leaving the NPC by permanently fusing it to its interaction partner Nup159 ('Dbp5 tether', Dbp5-$^{\Delta N}$Nup159, (Adams and Wente, 2020)), Nab2 focus formation was strongly reduced and the mobility of Nab2 was only mildly affected in long-term glucose withdrawal (Fig. 3I-K and S3I). This suggests that reduction of Dbp5 abundance at the NPC in response to glucose starvation is required for Nab2 focus formation.

We conclude that, upon glucose starvation, RNA-dependent Nab2 focus formation correlates with reduction of Dbp5 abundance at the NPC to facilitate bulk mRNA retention in the nucleus.

Protein-protein dimerization, but not predicted IDRs, drives Nab2 condensation

Nab2 is predicted to contain several IDRs including an RGG and a polyQ domain (Fig. S2H). To identify the domains in Nab2 that are responsible for the alterations in nuclear dynamics in glucose stress, we tested the effect of IDR domain removal on condensation behavior *in vitro*. Deleting the Q-rich domain did not abolish condensate formation, but slightly shifted the pH-dependency to higher pH values (Fig. S5A). Deleting the RGG domain and replacing it with an exogenous nuclear import signal (ΔRGG^{SV40NLS}, with the SV40NLS replacing the endogenous NLS found in the RGG domain) also affected the pH sensitivity of Nab2, which was even more pronounced than for Nab2$^{\Delta Q}$-GFP (Fig. S5A). Surprisingly, when both domains were deleted (Nab2$^{\Delta Q\text{-}\Delta RGGSV40NLS}$-GFP, 'IDR mutant'), condensates could still form, even though the major regions expected to be critical for condensation were removed. In addition, droplets with this Nab2 variant formed even in the absence of RNA (Fig. 4A) and were less dynamic and more solid-like compared to their wild type counterparts, as shown by a reduction in recovery by FRAP (Fig. 4B). We then tested a Nab2 variant that has been previously been shown to affect mRNA compaction by impairing Nab2 dimerization on RNA (Nab2^{F450A}, (Aibara et al., 2017)). Intriguingly, this Nab2 dimerization mutant displayed a strong reduction in condensate formation (Fig. 4A). Thus, our results suggest that Nab2 condensate formation does not require the IDRs but instead depends on the protein's ability to dimerize on RNA. Furthermore, the major disordered regions within the protein, in particular the RGG domain, help to keep Nab2 condensates dynamic.

The type of Nab2 condensate determines the degree of nuclear mRNA retention

How does the ability of Nab2 to undergo phase separation affect nuclear focus formation and RNA retention *in vivo*? Whereas the expression of a Nab2 variant that lacks the Q-rich domain (ΔQ) did not result in any growth disadvantages, deletion of the RGG domain (ΔRGG^{SV40NLS}) led to a severe growth impairment (Fig, S5B). Intriguingly, the combined deletion of both the Q and the RGG domain (ΔQ-ΔRGG^{SV40NLS}, IDR mutant) rescued the growth defect of the ΔRGG^{SV40NLS} mutant (Fig. S5B), and we therefore continued our experiments with this mutant (Fig. S5C). Consistent with our *in vitro* results, both Nab2^{ΔQ}-GFP and Nab2$^{ΔQ\text{-}ΔRGG\text{-}SV40NLS}$-GFP still formed foci in the nucleus upon long-term glucose starvation (Fig. 4C and Fig. S5E) coinciding with a reduction in nuclear mobility compared to WT in FRAP (Fig. 4D,E and Fig. S5F,G). In contrast, the dimerization mutant Nab2^{F450A} formed almost no nuclear foci (Fig. 4C) and also did not show a reduction in nuclear mobility (Fig. 4F). This suggests that the degree to which Nab2 mutants form condensates *in vitro* reflects focus formation and nuclear mobility *in vivo*.

Intriguingly, Nab2's ability to form foci in stress is also linked to its ability to retain RNA in the nucleus: while the IDR mutant showed an increased nuclear poly(A) RNA signal, the dimerization mutant displayed decreased nuclear poly(A) RNA retention during stress (Fig. 5A,B). This implies that the level of Nab2 condensate formation determines the degree of nuclear RNA retention in long-term glucose starvation. Of note, the Nab2 IDR mutant also showed a slight nuclear mRNA retention phenotype even in log growing cells (Fig. 5A and S5H), suggesting that the RGG domain is important for efficient mRNA export both in unstressed and stressed cells.

Nab2 condensation confers selective RNA retention in stress and is critical for survival after prolonged stress

In order to identify which mRNAs are retained in nuclear Nab2 foci in stress and to examine if this altered in the Nab2 mutant backgrounds (Nab2$^{ΔQ\text{-}ΔRGGSV40NLS}$-GFP and Nab2^{F450A}-GFP) we next purified poly(A)-RNA from whole cells cultured in +glucose and 24 hrs –glucose conditions, as well as from nuclear fractions of cells starved for 24 hrs in –glucose (Fig. S5J,K and Supplementary Table 4). As expected, we detected a global rearrangement of the transcriptional landscape between the +glucose and 24 hrs –glucose conditions on a whole cell level, (Fig. S6A). This is in agreement with RNA FISH quantifications that revealed a 5-fold reduction of total poly(A) RNA abundance in 24 hrs –glucose compared to +glucose (Fig. S5I). However, for a given condition, the RNA sequencing reads of the wild type and the mutants did not differ (Fig. S6A) and a stress response was initiated to a similar extent in all strains at the total RNA level (Fig. S6B). By contrast, differences in the nuclear RNA fractions could be observed between the wild type and the Nab2 mutants in 24 hrs –glucose revealing an increase in sequencing reads (CPM, counts per million) for the IDR mutant Nab2$^{ΔQ\text{-}ΔRGGSV40NLS}$ compared to wild type, whereas the dimerization mutant Nab2^{F450A} did not significantly differ from the wild type (Fig. 5C and S6D). Intriguingly, the IDR mutant displayed selective nuclear enrichment of certain transcripts whereas others did not show any differential enrichment (Fig. 5C). Gene ontology (GO) term analysis of the most abundant transcripts (CPM >500 in Nab2-GFP average of 3 replicates (318 genes) representing 42% of the total reads; Fig. 5C (blue dots), Fig. 5D (purple) and Fig. S6F,G) revealed that the highest-scoring GO terms for differentially enriched transcripts were stress response-related (protein folding, cellular response to oxidative stress/heat, cellular oxidant detoxification), and carbohydrate metabolic processes. Transcripts that were not differentially enriched fraction (Fig. 5D, grey) showed highest-scoring GO terms in translation, translation termination, glycolytic process/gluconeogenesis and rRNA binding (i.e. 'pro-proliferation' mRNAs). To confirm our RNA sequencing results, we performed RNA

FISH experiments using probes against individual mRNAs that either belong to the class of differentially enriched mRNAs (*BTN2, HSP42, HXT6*, Fig. 6A-F and Fig. S6H) or to the not differentially enriched mRNAs (*DED1*, Fig. 6G,H and Fig. S6H). Indeed, these experiments confirmed nuclear RNA retention and condensate selectivity for the tested transcripts.

Our results reveal that wild type Nab2 retains pro-proliferation mRNAs in the nucleus that are not induced in stress allowing the selective export of stress-induced mRNAs (Fig. 6). The altered condensate state seen in the IDR mutant Nab2$^{\Delta Q\text{-}\Delta RGGSV40NLS}$ prevents the selective transport of stress-induced mRNAs, which results in their nuclear accumulation.

Finally, we also asked whether there is a physiological consequence of the altered mRNA retention in long-term stress. We therefore washed cells acutely into medium without glucose and incubated them for 5 days before allowing them to recover on rich medium plates containing glucose. Compared to wild type, the IDR mutant Nab2$^{\Delta Q\text{-}\Delta RGGSV40NLS}$ displayed a slight growth disadvantage on rich medium plates in log growing cells, which was exacerbated after prolonged glucose withdrawal (Fig. 7A) and when stress is maintained after dextrose recovery by incubating cells at different temperatures (Fig. 7A and S7A). Furthermore, gradual glucose depletion also affected the recovery of the IDR mutant as cells that had recovered from early stationary phase (24 hrs after mid-log phase) showed a similar growth impairment as after acute glucose withdrawal (Fig. S7B).

In summary, our results suggests that aberrant mRNA localization caused by altered Nab2 condensation affects survival in and recovery from glucose stress conditions.

Discussion

Here we show that the mRNA export factor Nab2 can form biomolecular condensates *in vitro* and *in vivo*, which are counteracted by the activity of the DEAD-box ATPase Dbp5. Our results provide evidence that the nuclear RNA-dependent Nab2 condensates globally retain bulk mRNAs in the nucleus in physiologically relevant stress conditions. Furthermore, our results suggest that a group of stress-induced mRNAs can bypass nuclear accumulation and predominantly localize in the cytoplasm. Based on these results, we propose a model in which stress-related transcripts can escape nuclear retention to elicit a timely cellular stress response, suggesting that cells use selective confinement in or release from nuclear condensates to re-wire mRNA export during stress (Fig. 7B). Nuclear-retained mRNAs largely represent pro-proliferation transcripts, which remain intact as both the cap-binding complex as well as the poly(A)-binding protein Nab2 enrich in stress-induced nuclear RNA foci, suggesting that the mRNA cap and poly(A) tail are still present (Fig. 5C,D). Storing them in the nucleus during glucose starvation might be a cellular strategy required for re-initiation of cell growth after stress release, allowing cells to quickly re-start protein production in a transcription-independent fashion, minimizing energy consumption at early stages of re-growth. Nuclear retained mRNAs tend to be longer (Fig. S6I) and more likely stem from intron-containing genes (Fig. S6J) than mRNAs that evade nuclear retention (e.g., those induced in glucose stress, Fig. 5D), although it is unclear if those mRNAs still contain introns once they are present in nuclear Nab2 condensates. Nab2 has been implicated in splicing regulation and artificial depletion of Nab2 from the nucleus leads to transcriptional read-through which produces chimeric transcripts with retained introns (Alpert et al., 2020; Soucek et al., 2016). RNA length has been reported to correlate with enrichment in cytoplasmic stress granules and poor translation efficiency (Khong et al., 2017), suggesting that short transcripts, such as mRNAs responsible for the cellular stress response, could evade both nuclear and cytoplasmic condensates to allow for their preferential translation in stress conditions. Furthermore, nuclear mRNA retention has previously been reported in mammalian systems, where it

serves to rapidly modify the neuronal transcriptome upon stimulation (Mauger et al., 2016), or to buffer gene expression noise (Bahar Halpern et al., 2015). Buffering mechanisms could also be at play in yeast, which needs to be investigated in the future.
The other tested mRNA-binding proteins, Yra1 and Npl3, do not enrich in Nab2 condensates (Fig. S3C,D), and this selective exclusion could hint towards nuclear remodeling of mRNPs in stress conditions, which could in turn facilitate bulk nuclear mRNA storage. Since their nuclear mobility does not change in unstressed versus stress cells (Fig. S3E-H), Yra1 and Npl3 could still dynamically associate with a subset of mRNAs in stress that are excluded from the Nab2 condensate, e.g., stress-induced mRNAs, which could be a requirement for their swift and efficient nuclear export. Future research is needed to understand mRNP composition and its functional consequence in long-term glucose stress.

We show that Nab2 condensate formation is regulated by the activity of Dbp5 (Fig. 2D and Fig. S2M), and that forcing Dbp5 to nuclear pore complexes (NPCs) via fusion to $^{\Delta N}$Nup159 prevents stress-induced Nab2 mobility reduction and nuclear focus formation (Fig. 3I-K). Previous reports have demonstrated a transient Nab2 and Dbp5 interaction at the NPC using a splitVenus system (Adams and Wente, 2020). We speculate that the DEAD-box ATPase Dbp5 could generally act to dissolve RNA-containing condensates. Consistent with this, overexpression of the mammalian ortholog of Dbp5, DDX19, prevents stress granule formation in an RNA binding-dependent manner (Hochberg-Laufer et al., 2019; Tauber et al., 2020). However, local ATPase activation through its interaction partner Gle1, which resides exclusively at the NPC, could target Dbp5's activity largely towards specific RNPs such as Nab2-bound mRNAs that pass the NPC during export. In line with this, Dbp5-$^{\Delta N}$Nup159 localization has been shown to be sufficient for viability (Adams and Wente, 2020), suggesting that the essential role of Dbp5 is restricted to the NPC.

Nuclear Nab2 condensation depends on several domains that modulate the degree of condensation and the material properties of the condensates, thereby controlling the degree of nuclear RNA retention (Fig. 5A,B). Surprisingly, when we deleted the major regions predicted to be causal for condensation (Fig. S2H), the Q-rich domain and the RGG domain, we observed a stronger Nab2 condensation phenotype, indicating that these domains act together to function as 'liquefiers' of condensates or to block condensation altogether. Similar observations have been made for the stress granule component Ded1, where deletion of evolutionarily preserved residues in its N-terminal intrinsically disordered region (IDR) lead to constitutive SG formation (Iserman et al., 2020). How these two domains act together to facilitate proper Nab2 condensation is unclear. Their relative position within the protein structure might be important, and the presence of an RGG domain could provide a survival benefit when the protein also contains a Q-rich domain, as deletion of the Nab2 RGG domain alone is lethal, while co-deleting the Q-rich domain restores growth (Fig. S5B). Spatial domain organization has previously been shown to affect condensate formation, as placing a Q-rich region close to the RRM of G3BP1 restored SG formation (Yang et al., 2020).
Conversely, Nab2 condensation (and nuclear focus formation/RNA retention) depends on its ability to dimerize on RNA (Nab2^{F450A}, Fig. 4A,C and 5A). The dimerization mutation lies within the zinc fingers (ZnF) essential for RNA binding, highlighting the multivalent binding mode of Nab2 as well as the importance of non-IDR regions for condensate formation. Indeed, Yang *et al.* have previously shown that increasing the number of ZnFs promotes cytoplasmic condensation of the SG component G3BP1, highlighting how altering RNA binding strength and potentially the valency of interaction affects condensate formation (Yang et al., 2020).

Glucose starvation is accompanied by an intracellular pH drop from pH 7.5 to approximately pH 6-6.5 (Dechant et al., 2014; Joyner et al., 2016; Martínez-Muñoz and Kane, 2008; Orij et al., 2009). Intriguingly, altered condensation of the IDR mutant Nab2$^{\Delta Q\text{-}\Delta RGGSV40NLS}$ resulted in pH insensitivity *in vitro* (Fig. 4A) and a slight nuclear enrichment of poly(A) RNA even in +glucose conditions (Fig. 5A and Fig. S5H), suggesting that Nab2 condensation could also play a role in mRNA export in exponentially growing cultures. Future research is needed to determine the extent to which mRNP (micro)condensation is also involved in mRNA export in unstressed cells, and if the essential function Dbp5 in mRNA export is to locally prevent or modulate mRNP condensation.

Materials and Methods

Supplemental Table 1 (Strain list)

Strain name	Genotype	Figure	Reference
KWY6116	*MAT A his3⊿1 leu2⊿0 ura3⊿0 NDC1::NCD1-yomKate2-URA3 GFA1::GFA1-24xPP7stemloops::loxP-kan*R*-loxP pMET25-PP7CP-yEGFP::LEU2*	1B,C	This study
KWY6353	*MAT A his3⊿1 leu2⊿0 ura3⊿0 NDC1::NCD1-yomKate2-URA3 GFA1::GFA1-24xPP7stemloops pMET25-PP7CP-yEGFP::LEU2*	1B,C	This study
KWY8262	*MAT A leu2 his3 NAB2::NAB2-yEGFP-URA3 DBP5::DBP5-3V5-IAA7-KANMX trp1-1:: ds*Red*-HDEL*	1D-H	This study
KWY8263	*MAT alpha leu2 NAB2::NAB2-yEGFP-URA3 DBP5::DBP5-3V5-IAA7-KANMX trp1-1:: ds*Red*-HDEL HIS::pGPD1-os*TIR*-HIS*	1D-H	This study
KWY8258	*MAT A leu2 his3 NAB2::NAB2-yEGFP-URA3 DBP5::DBP5-3V5-IAA7-KANMX RPB2::RPB2-3V5-IAA7-KANMX trp1-1:: ds*Red*-HDEL*	1G,H	This study
KWY8395	*MAT A leu2 his3 NAB2::NAB2-yEGFP-URA3 DBP5::DBP5-3V5-IAA7-KANMX RPB2::RPB2-3V5-IAA7-KANMX trp1-1:: ds*Red*-HDEL pNH603-pGPD1-os*TIR*::HIS*	1G,H	This study
KWY6567	*MAT alpha his3-11,15 trp1-1 ura3-1 ade2-1 DBP5::DBP5-link-yEGFP::Ca*URA3 *TRP1:: ds*Red*-HDEL*	3A,B S3A,B S3I	Rajoo *et al.* PNAS 2018
KWY9296	*MAT alpha his3Δ1 leu2Δ0 lys2Δ0 ura3Δ0 NAB2::NAB2-yEGFP-HISMX*	3C-H, 4C,D,G 5A-C 6A-H 7A S4A-F S5C,D,H-K S6A-J S7A,B	This study
KWY9399	*MAT alpha his3Δ1 leu2Δ0 lys2Δ0 ura3Δ0 NAB2::NAB2-ΔQQQP-ΔRGG(Δ104-263)-SV40NLS-yEGFP-HISMX*	4C,E,G 5A-C 6A-H 7A S5C,H-K S6A-J S7A,B	This study
KWY9823	*MAT alpha his3Δ1 leu2Δ0 lys2Δ0 ura3Δ0 NAB2::NAB2-F450A-GFP-HISMX*	4C,F,G 5A-C 6A-H 7A S5D,H-K S6A-H,G S7A,B	This study
KWY10392	*MAT A his3-11,15 ura3-1 leu2-3 trp1-1Nab2-GFP::HIS*	3I-K	This study
KWY10394	*ura3-1 his3-11 leu2-3 dbp5Δ::KAN nup159Δ::KAN pDBP5-NUP159ΔN::LEU NAB2::NAB2-GFP-HIS*	3I-K	This study

KWY7462	*MAT alpha TRP1::dsRed-HDEL DBP5::DBP5-GFP-IAA7-KANMX pNH603-pGPD1-osTIR::HIS*	S1A	This study
KWY6037	*MATalpha his3-11,15 trp1-1 ura3-1 ade2-1 NUP84::NUP84-link-yEGFP::CaURA3 TRP1::dsRed-HDEL*	S1C	Rajoo *et al.* PNAS 2018
KWY6041	*MATalpha his3-11,15 trp1-1 ura3-1 ade2-1 NUP133::NUP133-link-yEGFP::CaURA3 TRP1::dsRed-HDEL*	S1C	Rajoo *et al.* PNAS 2018
KWY6048	*MATalpha his3-11,15 trp1-1 ura3-1 ade2-1 NUP82::NUP82-link-yEGFP::CaURA3 TRP1::dsRed-HDEL*	S1C	Rajoo *et al.* PNAS 2018
KWY6053	*MATalpha his3-11,15 trp1-1 ura3-1 ade2-1 NUP60::NUP60-link-yEGFP::CaURA3 TRP1::dsRed-HDEL*	S1C	Rajoo *et al.* PNAS 2018
KWY6054	*MATalpha his3-11,15 trp1-1 ura3-1 ade2-1 NUP159::NUP159-link-yEGFP::CaURA3 TRP1::dsRed-HDEL*	S1C S3A,B	Rajoo *et al.* PNAS 2018
KWY6921	*MATalpha his3-11,15 trp1-1 ura3-1 ade2-1 NUP159::NUP159-link-yEGFP::CaURA3 TRP1::dsRed-HDEL DBP5::DBP5-GFP-IAA7-KANMX*	S1C	This study
KWY7056	*MATalpha his3-11,15 trp1-1 ura3-1 ade2-1 NUP159::NUP159-link-yEGFP::CaURA3 TRP1::dsRed-HDEL DBP5::DBP5-GFP-IAA7-KANMX pNH603-pGPD1-osTIR::HIS*	S1C	This study
KWY7407	*MATalpha his3-11,15 trp1-1 ura3-1 ade2-1 NUP133::NUP133-link-yEGFP::CaURA3 TRP1::dsRed-HDEL DBP5::DBP5-GFP-IAA7-KANMX*	S1C	This study
KWY7408	*MATalpha his3-11,15 trp1-1 ura3-1 ade2-1 NUP82::NUP82-link-yEGFP::CaURA3 TRP1::dsRed-HDEL DBP5::DBP5-GFP-IAA7-KANMX*	S1C	This study
KWY7412	*MATalpha his3-11,15 trp1-1 ura3-1 ade2-1 NUP60::NUP60-link-yEGFP::CaURA3 TRP1::dsRed-HDEL DBP5::DBP5-GFP-IAA7-KANMX*	S1C	This study
KWY7444	*MATalpha his3-11,15 trp1-1 ura3-1 ade2-1 NUP133::NUP133-link-yEGFP::CaURA3 TRP1::dsRed-HDEL DBP5::DBP5-GFP-IAA7-KANMX pNH603-pGPD1-osTIR::HIS*	S1C	This study
KWY7446	*MATalpha his3-11,15 trp1-1 ura3-1 ade2-1 NUP82::NUP82-link-yEGFP::CaURA3 TRP1::dsRed-HDEL DBP5::DBP5-GFP-IAA7-KANMX pNH603-pGPD1-osTIR::HIS*	S1C	This study
KWY7458	*MATalpha his3-11,15 trp1-1 ura3-1 ade2-1 NUP60::NUP60-link-yEGFP::CaURA3 TRP1::dsRed-HDEL DBP5::DBP5-GFP-IAA7-KANMX pNH603-pGPD1-osTIR::HIS*	S1C	This study
KWY8118	*MAT A his3⊿1 leu2⊿0 met15⊿0 ura3⊿0 TRP1::dsRed-HDEL-natMX DBP5::DBP5-3V5-IAA7-KANMX xpo1⊿::HYGMX pRS313-XPO1(LMBsensitive)::HIS3MX pADH1-NLS-NES-2xGFP::URA3*	S1B,D-G	This study
KWY10381	*MAT A his3⊿1 leu2⊿0 met15⊿0 ura3⊿0 TRP1::dsRed-HDEL-natMX DBP5::DBP5-3V5-IAA7-KANMX xpo1⊿::HYGMX pRS313-XPO1(LMBsensitive)::HIS3MX pADH1-NLS-NES-2xGFP::URA3 pNH605-pGPD1-osTIR::LEU2*	S1D-G	This study
KWY9559	*MAT alpha his3Δ1 leu2Δ0 lys2Δ0 ura3Δ0 NAB2::NAB2-yEGFP-HISMX DBP5-3V5-IAA7::KANMX*	S1H	This study
KWY9579	*MAT alpha his3Δ1 leu2Δ0 lys2Δ0 ura3Δ0 NAB2::NAB2-yEGFP-HISMX DBP5-3V5-IAA7::KANMX LEU2::pNH605-pGPD1-osTIR1*	S1H, S2G	This study
KWY7642	*MAT A his3⊿1 leu2⊿0 met15⊿0 DBP5::DBP5-3V5-IAA7-KANMX YRA1::yEGFP-YRA1-NATMX*	S2A,B	This study
KWY7652	*MAT A his3⊿1 leu2⊿0 met15⊿0 DBP5::DBP5-3V5-IAA7-KANMX YRA1::yEGFP-YRA1-NATMX TRP1::pGPD1-osTIR-hphNT1*	S2A,B	This study
KWY8009	*MAT A his3⊿1 leu2⊿0 met15⊿0 TRP1::dsRed-HDEL-NATMX*	S2C,D	This study

	DBP5::DBP5-3V5-IAA7-KANMX NPL3::NPL3-yEGFP-URA3		
KWY8010	*MAT A his3⊿1 leu2⊿0 met15⊿0 TRP1::dsRed-HDEL-NATMX DBP5::DBP5-3V5-IAA7-KANMX NPL3::NPL3-yEGFP-URA3 pNH603-pGPD1-osTIR::HIS*	S2C,D	This study
KWY7855	*MAT A his3⊿1 leu2⊿0 met15⊿0 ura3⊿0 TRP1::dsRed-HDEL-natMX DBP5::DBP5-3V5-IAA7-KANMX p(PHO4-NLS-GFP3 ::URA3)*	S2E,F	This study
KWY7949	*MAT A his3⊿1 leu2⊿0 met15⊿0 ura3⊿0 TRP1::dsRed-HDEL-natMX DBP5::DBP5-3V5-IAA7-KANMX HIS::pNH603-pGPD1-osTIR p(PHO4-NLS-GFP3 ::URA3)*	S2E,F	This study
KWY8259	*MAT alpha leu2 NAB2::NAB2-yEGFP::URA3 DBP5::DBP5-3V5-IAA7::KANMX RPB2::RPB2-3V5-IAA7-KANMX trp1-1::dsRed-HDEL-TRP1 HIS::pGPD1-osTIR-HIS*	S2G	This study
KWY8050	*MATalpha his3-11,15 trp1-1 ura3-1 ade2-1 DHH1::DHH1-yEGFP-URA3*	S2I,J	This study
KWY8650	*MAT A his3⊿1 leu2⊿0 met15⊿0 ura3⊿0 TRP1::dsRed-HDEL-URA3 NAB2::NAB2-yEGFP-HIS3*	S2I,J S5B	This study
KWY6051	*MATalpha his3-11,15 trp1-1 ura3-1 ade2-1 GLE1::GLE1-link-yEGFP::CaURA3 TRP1::dsRed-HDEL*	S3A,B	Rajoo *et al.* PNAS 2018
KWY6268	*MAT A his3⊿1 leu2⊿0 met15⊿0 YRA1:: NATMX-yEGFP-YRA1*	S3C,E,F	This study
KWY8008	*MAT A his3⊿1 leu2⊿0 met15⊿0 TRP1::dsRed-HDEL-NATMX DBP5::DBP5-3V5-IAA7-KANMX NPL3::NPL3-yEGFP-URA3*	S3D,G,H	This study
KWY10277 (SWY6285)	*MAT A ura3-1 his3-11 leu2-3 dbp5Δ::KAN nup159Δ::KANN GFP-DBP5-NUP159ΔN::LEU*	S3I	Adams & Wente, PLoS Genetics 2020
KWY7690	*MAT A his3⊿1 leu2⊿0 met15⊿0 CBC2::CBC2-GFP(S65T)-HIS3MX*	S4G	Huh *et al.* Nature 2003
KWY7696	*MAT A his3⊿1 leu2⊿0 met15⊿0 CBC1::CBC2-GFP(S65T)-HIS3MX*	S4G	Huh *et al.* Nature 2003
KWY8215	*MAT alpha his3⊿1 leu2⊿0 ura3⊿0 TRP1::dsRed-HDEL-natMX NAB2::NAB2-GFP-Y66L-IAA7-KANMX pNH603-pGPD1-osTIR::HIS*	S5B	This study
KWY9288	*MAT alpha his3⊿1 leu2⊿0 ura3⊿0 TRP1::dsRed-HDEL-natMX NAB2::NAB2-GFP-Y66L-IAA7-KANMX pNH603-pGPD1-osTIR::HIS p(Nab2-yEGFP-LEU2 (CEN))*	S5B	This study
KWY9289	*MAT alpha his3⊿1 leu2⊿0 ura3⊿0 TRP1::dsRed-HDEL-natMX NAB2::NAB2-GFP-Y66L-IAA7-KANMX pNH603-pGPD1-osTIR::HIS p(Nab2-ΔRGG(Δ201-263)-SV40NLS-yEGFP-LEU2 (CEN))*	S5B	This study
KWY9290	*MAT alpha his3⊿1 leu2⊿0 ura3⊿0 TRP1::dsRed-HDEL-natMX NAB2::NAB2-GFP-Y66L-IAA7-KANMX pNH603-pGPD1-osTIR::HIS p(Nab2-ΔQQQP-ΔRGG(Δ104-263)-SV40NLS-yEGFP-LEU2 (CEN))*	S5B	This study
KWY8666	*MAT A his3Δ1 leu2Δ0 lys2Δ0 ura3Δ0 TRP1::dsRed-HDEL-natMX NAB2-ΔQQQP(Δ104-169)-yEGFP-HISMX*	S5C	This study
KWY10234	*MAT? his3Δ1? leu2Δ0? met15Δ0? lys2Δ0? ura3Δ0 NAB2-ΔQQQP(Δ104-169)-yEGFP-HISMX*	S5E-G	This study

Supplemental Table 2 (Plasmid List)

Plasmid name	description	Figure	Published

pKW2499	6xHIS-TEV-ΔN90-Dbp5 (KAN)	2C	Montpetit *et al.* Nature 2011
pKW2501	6xHIS-TEV-ΔN90-Dbp5-DQAD (KAN)	2C	This study
pKW3714	6xHis-V5-Dbp5-mCherry (AMP)	S5B	This study
pKW4404	6xHis-V5-Gle1 s.c. [244-538] (AMP)	S5B	This study
pKW4814	6xHis-TwinStrep-PreScission-Nab2-yEGFP (AMP)	2A-C 4A S5B-D	This study
pKW4817	6xHis-TwinStrep-PreScission-Nab2-ΔRGG(Δ201-263)-SV40NLS-yEGFP (AMP)	S8G	This study
pKW4818	6xHis-TwinStrep-PreScission-Nab2-ΔQQQP-ΔRGG(Δ104-263)-SV40NLS-yEGFP (AMP)	4A	This study
pKW4954	6xHis-TwinStrep-PreScission-Nab2-F450A-yEGFP (AMP)	4A	This study
pKW4957	6xHis-TwinStrep-PreScission-Nab2-ΔQQQP(Δ104-169)-yEGFP (AMP)	S8G	This study

Supplemental Table 3 (Oligo list (smFISH))

Oligo	Sequence	Modification	Company
dT30	TTT TTT TTT TTT TTT TTT TTT TTT TTT TTT	TAMRA (3' end)	Microsynth
BTN2	1 GGCAGCTGTTCAAAAACACA 2 CGAATGTAGGGGCTGACTAA 3 ATAGCTCACTGGAGAACTGC 4 TTTCCTCCTTTTACATTCTG 5 GCTCTTAGGTTAGCTTTTAT 6 ATTTGCATCGCTTTTTTTTG 7 TGCATACCTCAAAGGTTCTG 8 TAACCATTTGGTGTTTCAGC 9 GTTCATATGGAATCCGCTTA 10 ACCTAATTTCTCATTAACGT 11 TGTAATGGTTCTCCTTTAGC 12 TCTTGGACAACATGGTAAGT 13 TCCGCTTCATCTTCAACATA 14 GCAGATCTCAATAGAGCATC 15 GGCTCTAAAATCCAGATCTT 16 TCCTTAGCAATTTTCTTTCC 17 TTCTATTTCGTAGTCTTGGA 18 ATTCATCACCTCTATGATTC 19 TCCTTCTTACTCAATATGCT 20 CTTGGTCTAGAGAGAATTCC 21 CAACTCCACAGCCAATAACA 22 ATATTTTTCTCTCGAGCCAT 23 CCTCATGCTTAACTAAACCA 24 ATGCCACCTTCGGAAATTTC 25 TTATTGGCATCTTTGGTTCG 26 GACTCGTCTATTTTGGATTC 27 AGACATGTTAACATCATCGT 28 CTTCTTCCTCCTTCAAAGAT	Cal Fluor Red 590 (3' end)	BioCat

	29 TTTGGTTAGTGGTTCTTTCG 30 TCCATTTTTTTATTTGGTCT 31 TGCATCAATCTTTCTTCCTC 32 CTGTTCTGATTTTCTGCTTT 33 TTTTGCCTTTCTTCATCTTC 34 CAATCTGGCTTCCTTCTCTT 35 TCAAAGATTCTTTCCTTGCC 36 CTCTTGGTTTTTTGCTTATT 37 TTGCAATTTTTTTTGCTGGG 38 TCTCAGAGATAGGCAATGAT 39 TTATTTTTATTGCTGGCCTC 40 TATCACTTTCTGCTGAACCA 41 GTCGTATCAGAATCACTGTT 42 ACCAGACACAGAGAAATCCA 43 GAAGCGTGTTTTTTTAGTGT 44 CTCAACGTCTTCTAATAGGG 45 TGTATCTGTCAACTTCCTCA 46 GGAGATCTGCTTAGGGACTC 47 CCTCAATAATAGAGTTTCCC		
HSP42	1 AGAGATAGGGATGGTTGATA 2 CCAGTTTGGTTGGATAATGC 3 TTTGTGGTTGGCGAGGATAT 4 ACGTGCACTTGTCCATAATG 5 ATGATGACGAGGATGATGCC 6 AGGAACACCATTGTATCTGC 7 TCCAGGGAACTGGTAGTAAT 8 CAGGACTATAGTAATAGGCT 9 ACCATCCTCGTCATCATAAC 10 ACCATATCTTCGTCTTGGTC 11 CATCTTCCTGTCTTGTAGTG 12 TGGATATCTTCTCGAGTTGC 13 TCCTGGCAGTATTACAATGG 14 CGTTTAAACTGTTTGCCTGT 15 GAACACCTATTAACGCGGTT 16 TGGTTCAGTGCCTTCATATG 17 CTGTTCGGTATTTGCTTCAA 18 TTCTTATCCTTTTCTTCTCC 19 TTTGGGTGCTTCAGACTTAT 20 TTTTTCTTTGTTGGTTTCGC 21 ATTCCTCCAGCTGATTCAAA 22 TTTTTTGGCTAATGGTGGTC 23 TGTAGGTGAGCGAACGATGA 24 GTCAGGTATTGGGGAAGGCG 25 CAGGCTTGGATACTTGTAAC 26 AATGGTAAGTCCATTCTCGT 27 CATAGACATTCACTTCTGGT 28 AACTACGTAAGTGTCCTCGG 29 TAGCACCTGGTAACGCAAGA	Cal Fluor Red 590 (3' end)	BioCat

	30 TCAATGTGGAAAGCCCTAGA 31 CTCATGAGAAGATGGATGGT 32 TCGATCTTACCCTTGATGAG 33 TTTCATCAATGCCCACTCTG 34 AGTTCCGTGATCTTCAAGAA 35 TCTCTCAAACGCACCATATT 36 GCAGCACGGGGAATTTAACG 37 ATTTCTTCGTCCTTAATGCG 38 ACCGTTGTTGTAAGTAGCTT 39 TAGGCACCTTAATTTGTAGT 40 GCTTTTCAGTGTCATTGACA 41 AATGGCGATCCTCTTTTTTG 42 CAATTCTTCGTCGGGTATTT 43 CAATTTTCTACCGTAGGGTT		
HXT6	1 AGGAGTTTGCTCTGCAATAG 2 TCAACAGCAGAGAGATGCTC 3 GATAAAACCGAGTGGGAGGC 4 TCTTTCAGCCTTGTTTGATG 5 ACCTTCACCATAAGCTTTTA 6 CTGGTCTCTTTGGAATTTCA 7 GAGACAGTGACATAGGCAGA 8 ACGAAACCACCAAAGGCGAT 9 AAATGGTACCAGTATCCCAA 10 AGTACCATCTTTATGCTTCA 11 ACCAGTTCTAACCTTAGACA 12 CACCAATGGCACAACCAATG 13 CCGTACATATCACCCAATTT 14 CGACAATCAAACCCACCTTA 15 AACGGCAATACCACCAACAC 16 GCTTTGGGGATACTTCAGAA 17 CAAGAGACTAAAGTACCCCT 18 ACCGGCAGTAATCATCAATT 19 GTTGGTACAGTAACCCAAGA 20 TGGAGTAGTTCTTAGTACCG 21 ACCTAATGGAACTCTCCATT 22 TCATAAACAAAGCCCAGGCA 23 ACGTGGAGACTCTGGAACAA 24 TTCGATCTTACCGACTTCAG 25 ACGGCAATAGAACGTTTGGC 26 TGGATCATCAACAGCAACCT 27 AGCTTCGACTTCAGCCAAAA 28 TTACCAGCTAATTTCTCTGC 29 ACTAAACAATTCACCCCAGG 30 AAACGCTGAAGGACCTTTGT 31 TTGAATCATAGCACCCATGA 32 CACCTGTCAATTGTTGTAGA 33 ACTCAAACCAACAGCCTTGA 34 ACCCCATAGCAAACAAGTAC	Cal Fluor Red 590 (3' end)	BioCat

	35 TACAAGCAGTCATGGATGCA 36 ATTTGGCCATAATCTGGTGA 37 CTTGGAAGATGGTTGGTCTT 38 AGCCCATGTAGTAGCAAAAC 39 AGACTTGACTCTCAATGGGA 40 GCAGCTGTAGCAATAGACAT 41 TCAAGAAACCCCACAACCAA 42 CAGCCCATGAAAACGTAACC 43 CCCTTAGTTTCTGGAACAAC 44 TGGTGTTGACTTCTTCCAAA 45 CATGGTAGAACACCTTCTTC 46 TAGATGGTGGAACCCATGAG 47 TTATCATCGTGAGCCATTTC 48 TTTGGTGCTGAACATTCTCT		
DED1	1 AATTTTGCACTTGTTCGCTC 2 TAACCATTCTCGTTGTTGTC 3 GTTTTCCTCTTAAGTGAGGA 4 ACTGTTATTTCTGGCACTTC 5 CCGTTGTTGTTATTGTAGTT 6 TTGTTGCTAAAGAAGCTGCC 7 TTGTTTCCACCGAAGAAACC 8 CACCAAATATGGCGATCTCG 9 TGGAAATTTGGATCCTCGGG 10 CGTCCACTGGAATATCATCG 11 TGGTTCAGGAACATCCTTAC 12 TTCCAATAACAATCCGTCCA 13 TGGTGAAACGGGCCAATTTG 14 GGAGTATTTTTGCACAGGTG 15 TGATTCGGACAACACTGGGA 16 GAGACTCTGGTTGAGGAGAT 17 GGCCTTTCTTTGGTAAAAGG 18 TCTCTAGTTGGAGCCATAAT 19 ATCGAAAATTTGGGTGGCCA 20 TTGACCCAGGATCTATAAGT 21 TTACCAATTGGAGAACCACC 22 AGATCGCAACCACGTTCAAT 23 TTCAAACGACCTGGAGTAGC 24 TTTACCACGTTCCAACAAGT 25 TACTTGACGTTGGCCAAAGA 26 ATCAGCTTCATCTAGAACCA 27 GTTCGAAACCCATATCCAAC 28 CAGGAGTCATATCACAGTCT 29 ATCAGAGTTTGTCTTTCACC 30 TCAGCGGGAAAAGTAGCTGA 31 AATCACGGGCCAAATGTTGG 32 AACCGACTCTACCAACAGAC 33 AGGCTGACTTCTTATCTTGA 34 AGTCAAACCGTCAGTGGATG	Cal Fluor Red 590 (3' end)	BioCat

	35 TTGATCTGCCATTCTCTTAG 36 GCATGATCAGGAAATCGGTC 37 ATGAATGGCGGTAGCTCTAA 38 TTCTCTCTCAGATTGGGTAC 39 ACAGCTGTGGCAACCAATAA 40 ATAACGTGGGTGACGTTTGG 41 GACCAGTTCTACCAATTCTA 42 AAAAGGCAGTGGCAAGACCG 43 TCTTGGTTAGCTTCAGTCAA 44 CGTCCTTCAAGAATGATGGG 45 AATCTCTGTTGTTGTTGCGA 46 GAGTTATCTCTGCTTCTTGA 47 GAAGACTTGGAATCGCTACC 48 CACCACCAAGAAGAGTTGTT		

Yeast strain construction

Saccharomyces cerevisiae strains were constructed using standard yeast genetic techniques either by transformation of a CEN plasmid, a linearized plasmid, or of a PCR amplification product with homology to the target site (Longtine et al., 1998). All yeast strains expressing a GFP-tagged protein were tagged with a yeast-optimized monomeric EGFP version (A206K).

Nab2-ΔQ and Nab2-ΔQ-ΔRGG^{SV40NLS} mutant strains were constructed using a CRISPR/Cas9 strategy (Laughery et al., 2015). In brief, gRNA sites were determined using Benchling (settings: single guide of 20 nt length and an NGG PAM site (SpCas9, 3' side)). For both Nab2-ΔQ and Nab2-ΔQ-ΔRGG^{SV40NLS} the cut site lies within the Q-rich region (gRNA regions amplified off pML104 (Laughery et al., 2015): (A) 'upstream' gRNA: GTCCCTAGTTGTGGCTGAAGgttttagagctagaaatagcaagttaaaataaggctagtccg + cggaaacgctatacctccacc; (B) 'downstream' gRNA: gcgaggaagcggaagagcg + ctagctctaaaacCTTCAGCCACAACTAGGGACgatcatttatctttcactgcggagaag; KWY9296 was transformed with stitched gRNA regions, SwaI-digested pML104 and PCR amplification products with homology to the target site (ΔQ: amplified homology product from genomic DNA excluding DNA region coding for aa104-169; -ΔQ-ΔRGG^{SV40NLS} amplified homology product from plasmid pKW4774 where DNA region coding for aa104-263 was replaced by SV40NLS sequence (AAAGGCCTAAGAAGAAGAGGAAAGTATTA)).

Yeast Cell Culturing

Cells were cultured in synthetic complete media containing 2% glucose (Formedium, CSC0205) (for microscopy, RNA FISH and nuclear extraction assay). Cells were inoculated from saturated overnight cultures into fresh medium and grown at 25°C to OD_{600} 0.6–0.8. For acute glucose withdrawal, cells were then washed 3 times in synthetic complete media without glucose, resuspended in the same medium and cultured for the indicated time (30 min or 24 hours).

Acute degron depletion was performed by addition of auxin (500 µM indole-3-acetic acid (IAA); 500 mM stock in ethanol) for the indicated time points (typically 1 or 2 hours). As a solvent control, cells were treated with ethanol.

Single-molecule fluorescence *in situ* hybridization (smFISH)

Probe design: DNA probes coupled to CAL Fluor Red 590 (Stellaris Biosearch Technologies, synthesized by BioCat) were used for smFISH, targeting gene-specific moieties for single molecule visualization. *dT30*

DNA probes coupled to TAMRA (synthesized by Microsynth AG) targeting poly(A) stretches were used for poly(A) RNA visualization.
Methodology: Samples were processed as described in (Derrer et al., 2019). Briefly, cultures were fixed for 30 min with 4% paraformaldehyde (Electron Microscopy Sciences, 15714). Cells were washed once with buffer B (1.2 M sorbitol and 100 mM KHPO4, pH 7.5, at 4°C), then spheroplasted for 20 min using 1% 20T zymolyase in 1.2 M sorbitol, 100 mM KHPO4, pH 7.5, 20 mM vanadyl ribonuclease complex (New England Biolabs, S1402S), and 20 µM β-mercaptoethanol. To stop the spheroplasting reaction, cells were washed once with buffer B, and then transferred into pre-hybridization buffer (10% formamide (Merck Millipore, S4117), 2x SSC (saline-sodium citrate buffer; Life Technologies, AM9624). Separately, 0.5 µL of probe mix (stock 25 µM) was mixed with 2 µL of salmon-sperm DNA (10 mg/ml; Life Technologies, 15632-011) and 2 µL yeast transfer RNA (10mg/ml; Life Technologies, AM7119). The probe mix was denatured in 50 µL of hybridization buffer F (20% formamide and 10mM NaHPO4, pH7.0) for 3 min at 95 °C, and then mixed with 50 µL hybridization buffer H (4x SSC, 4 mg/ml acetylated BSA (Sigma Fluka Aldrich, B8894-1.5mL), 20 mM vanadyl ribonuclease complex). This final hybridization mixture was added to the pre-hybridized cell pellet (which corresponds to approx. 3 OD_{600}) and incubated overnight at 37 °C. The next day, cells were washed in 1x PBS/DAPI and incubated for 3 min, washed again in 1x PBS and then stored at 4 °C.

Microscopy for live cell imaging and smFISH

For live cell imaging and NuRIM fluorescence intensity quantification experiments, cells were transferred to a 384-well plate (Brooks, Matrical MGB101-1-2-LG-L) treated with Concanavalin A (stock solution of 1 mg/ml, air-dried), and spun down for 1 min at 100 rcf.
For smFISH, approx. 1 OD_{600} of fixed cells were spread onto a glass slide using a 12mm cover slip (Huber, 10.0360.52) to obtain a single layer of cells prior to imaging. Alternatively, fixed cells were transferred to a 384-well plate (Brooks, Matrical MGB101-1-2-LG-L) treated with Concanavalin A (stock solution of 1 mg/ml, air-dried), and spun down for 1 min at 100 rcf, and washed twice with 1x PBS to obtain a single layer of cells.
All imaging experiments were performed at 25 °C. Microscopy was performed using an inverted epi-fluoresence microscope (Nikon Ti) equipped with a Spectra X LED light source and a Hamamatsu Flash 4.0 sCMOS camera using a 100X Plan-Apo objective NA 1.4 and NIS Elements software. For live cell imaging and smFISH image analysis, images were processed using FIJI software and plots were generated in GraphPad Prism 8 (GraphPad). For NuRIM quantification, images were processed using NuRIM code (Rajoo et al., 2018; Vallotton et al., 2019) in MATLAB. Briefly, this method uses the HDEL-DsRed signal to generate a mask that segments the nuclear envelope. This mask is then transferred to the GFP channel to extract average intensity information from this mask.

Fluorescence recovery after photobleaching (FRAP)

A) Yeast cells:
   200 µL of a culture with OD 0.6-0.8 was added to a Concanavalin A treated imaging well (IBIDI, µ-Slide 8-well, 80827), and spun down for 1 min at 100 rcf. Microscopy was performed on a Leica TCS SP8 STED/FLIM/FCS or a Leica TCS SP8-AOBS microscope using a 63x 1.4NA Oil HC PL APO CS2 objective. A bidirectional scanner at a speed of 8,000 Hz, NF488/561/633, an Airy unit of 1.5, and a FRAP booster for bleaching were applied for every FRAP experiment using a PMT detector (500–551 nm). An image size of 504 x 50 pixel and a zoom of 4 were used together with line accumulation of three, yielding a frame rate of 74.07 frames/s with a pixel dwell time of 73 ns. 50 prebleach and 300 postbleach frames were acquired. A 488-nm argon laser line was used at 30%

power. An elliptical region covering approximately one half of the cell nucleus was bleached. The bleaching was performed using 80% argon laser power for 195 ms. Imaging was conducted with 1.5% laser intensity (with a gain of 570 for Nab2-GFP and GFP-Yra1, and 560 for Npl3-GFP) to illuminate the GFP during prebleach and postbleach acquisition.

B) In vitro droplets:
Protein droplets were set up according to (Hondele et al., 2019). In brief, reactions were pipetted in 384-well microscopy plates (Brooks, Matrical MGB101-1-2-LG-L). 3 µL recombinant GFP-tagged protein (stock 150 µM to a final concentration of 20 µM) was mixed at room temperature with 20 µL of a master mix (14.5 µL LSB-100 (100 mM KCl, 30 mM HEPES-KOH pH 7.4, 2 mM $MgCl_2$), 0.9 µL CRM reconstitution mix (40 mM ATP, 40 mM $MgCl_2$, 200 mM creatine phosphate, 70 U ml−1 creatine kinase), 1.8 µL ATP/MgCl2 (100 mM), 0.9 µL BSA (10 mg mL−1), 0.9 µL poly(A) RNA (1 mg mL-1), 0.9 µL 1M HEPES pH 6.8, 0.1 µL RNasin Plus (Promega). Microscopy was performed on a Leica TCS SP8 STED/FLIM/FCS or a Leica TCS SP8-AOBS microscope using a 63x 1.4NA Oil HC PL APO CS2 objective. A bidirectional scanner at a speed of 8,000 Hz, NF488/561/633, an Airy unit of 1.5, and a FRAP booster for bleaching were applied for every FRAP experiment using a PMT detector (500–551 nm). An image size of 504 x 50 pixel and a zoom of 4 were used together with line accumulation of three, yielding a frame rate of 74.07 frames/s with a pixel dwell time of 73 ns. 50 prebleach and 800 postbleach frames were acquired. A 488-nm argon laser line was used at 30% power. Imaging was conducted with 1.5% laser intensity (with a gain of 570) to illuminate the GFP during prebleach and postbleach acquisition. The bleach was performed using 80% argon laser power for 195 ms. The bleaching was performed by defining an elliptical region covering approximately one half of the droplet.

C) Image analysis: 1) yeast cells: Fluorescence recovery in the bleached region was evaluated by subtracting the extracellular background from the intensity of the bleached region, and the values were then bleach-corrected by normalizing for total cell intensity (Bancaud et al., 2010). 2) droplets: Fluorescence recovery in the bleached region was evaluated by subtracting the background signal outside the droplet from the intensity of the bleached region, and the values were then bleach-corrected by normalizing for total droplet intensity. All curves were fitted with an exponential function in a custom-written MATLAB script. Plots were generated in GraphPad Prism 8 (GraphPad).

Nucleus extraction

The protocol was adapted from (Aris and Blobel, 1991) and (Niepel et al., 2017). Cells were inoculated in a 10 mL pre-culture of synthetic complete media containing 2% glucose (SCD, Formedium, CSC0205), and cultured for 8-10 hrs at 25 °C. Cells were then back-diluted in 500 mL SCD to OD_{600} 0.006, grown for 16-18 hrs at 25 °C to OD_{600} 0.8 and harvested onto a cellulose ester membrane filter (Whatman 10400921) using a vacuum filtration pump. Cells were then washed from the membrane with 40 mL ddH_2O into a 50 mL Falcon tube, spun down for 2 min at 845 rcf, resuspended in 25 mL buffer 1 (0.1M Tris-HCl pH7.4, 10mM DTT) and incubated shaking at 30 °C for 20 min in a horizontal shaker at 150 rpm. Cells were then spun down for 2 min at 845 rcf, washed in 10 mL buffer 2 (20mM KPi pH 7.4, 1.2M Sorbitol), and spun down again for 2 min at 845 rcf. For cell wall digestion (spheroplasting), cells were resuspended in 50 mL buffer 3 (20mM KPi pH 7.4, 1.2M Sorbitol, 10 mM ribonucleoside vanadyl complex (NEB S1402S, pre-warmed at 65 °C), 0.08mg/ml Zymolyase-20T (Amsbio 326921)) and incubated for 60 min at 30 °C in a rotation wheel. Spheroplasts were spun at 3000 rcf for 2 min, washed in 10 mL buffer 4 (20mM KPi pH 6.4, 1.2M Sorbitol), and spun again at 3000 rcf for 2 min. To release nuclei, spheroplasts were carefully resuspended in 20 mL buffer F (20% Ficoll, 20mM KPi pH 6.4, 5 mM

RVC, 0.005mg/ml Pepstatin A, 1x protease inhibitor cocktail (PIC, Sigma P8215-5mL), 250 µg/mL DAPI) and put on ice. To mechanically assist nuclei release, the lysate was then processed with 5 slow strokes in a dounce homogenizer on ice (this step is not essential as most of the nuclei are already released upon resuspension in buffer F). To separate nuclei from remaining cells/spheroplasts, the lysate was spun for 5 min at 3460 rcf at 4 °C. Afterwards, the supernatant was carefully removed with a 25 mL pipet until ca. 2 mL was left (to avoid pipetting the cell/spheroplast pellet) and transferred to a fresh 15 mL Falcon tube on ice. For nucleus enrichment and removal of other organelles, a sucrose gradient was prepared as follows: ice-cold 5 mL 2.5 M sucrose was added to the bottom of an open-top plastic tube (Beckman-Coulter 344058), carefully topped up with ice-cold 5 mL 1.875 M sucrose, which in turn was carefully topped up with ice-cold 5 mL 1.7 M sucrose. Lastly, the lysate supernatant was carefully added on top of the 1.7 M sucrose layer, and the full tube was transferred to a pre-cooled metal holder of a SW32Ti ultracentrifuge rotor (Beckman-Coulter). Tubes were spun for 30 min at 103.000 rcf at 4 °C, which resulted in 'cloudy' layer formation between the 1.7 M and 1.875 M sucrose interface (containing mostly cytoplasmic organelles, fraction 1) and between the 1.875 M and 2.5 M sucrose layer (containing nuclei, fraction 2). The enriched nucleus fraction 2 (typically around 4 mL) was then harvested by carefully pipetting away the top layers. To reduce the sucrose molarity, 4 mL of ice-cold buffer 5 (20mM KHPO4 pH 6.45) was added to the nucleus fraction 2, mixed and spun for 4 min at 3460 rcf at 4 °C. The supernatant was carefully removed with a 10 mL pipet until ca. 2 mL was left to separate any remaining cell debris from the nuclear fraction. 2x500 µL aliquots were taken for DNA content determination as a proxy for the amount of harvested nuclei. Enriched nuclei were then immediately processed for RNA extraction (see below).

RNA extraction from nuclear sucrose gradient fraction

The enriched nucleus fraction was transferred to a fresh open-top plastic tube (Beckman-Coulter 344058) and spun for 30 min at 20.000 rcf for 30 min in SW32Ti rotor. The pellet was resuspended in 500 µL RNase-free TES buffer (10 mM TrisHCl pH 7.5, 10 mM EDTA, 0.5% SDS) and transferred to screw-cap tubes. 500 µL acid-saturated phenol was added, the mixture was vortexed and incubated for 30 min in a thermo block at 65 °C (shaking at 150 rpm). Afterwards, the tube was put on ice for 5 min and then spun for 10 min at 13.000 rcf at 4 °C. The upper aqueous phase was transferred to a fresh RNase-free tube, mixed with 500 µL acid-saturated phenol, vortexed and spun for 5 min at 13.000 rcf at 4 °C. The upper aqueous phase was transferred to a chloroform-resistant screw-cap tube, mixed with 500 µL chloroform, vortexed and spun for 5 min at 13.000 rcf at 4 °C. The upper aqueous phase was transferred to a fresh RNase-free tube, mixed with 60 µL 3M NaOAc pH 5.2 and 700 µL isopropanol, and incubated overnight at -20 °C. The next morning, the mixture was spun for 40 min at 13.000 rcf at 4 °C, the supernatant was decanted and 300 µL 75% EtOH was added, followed by centrifugation for 5 min at 13.000 rcf at 4 °C. The supernatant was removed and the pellet was air-dried for 10 min on ice, resuspended in nuclease-free H2O and stored at -80 °C.

RNA extraction from whole cell lysates

Cells were inoculated in a 10 mL pre-culture of synthetic complete media containing 2% glucose (SCD, Formedium, CSC0205), and cultured for 8-10 hrs at 25 °C. Cells were then back-diluted in 400 mL SCD to OD_{600} 0.006, grown for 16-18 hrs at 25 °C to OD_{600} 0.8 and harvested onto a cellulose ester membrane filter (Whatman 10400921) using a vacuum filtration pump. Cells were scraped off the membrane with a metal rod and snap-frozen in a 50 mL Falcon tube containing liquid nitrogen. To lyse the cells, the cell pellet was resuspended in 400 uL TES buffer (10mM TrisHCl pH7.5, 10mM EDTA, 0.5% SDS), followed by addition of 400 uL acid-saturated phenol. The samples were incubated at 65°C for 1 hour

with constant vortexing. Afterwards, the tube was put on ice for 5 min and then spun for 10 min at 20.000 rcf at 4 °C. The upper aqueous phase was transferred to a fresh RNase-free tube, mixed with 500 µL acid-saturated phenol, vortexed and spun for 5 min at 20.000 rcf at 4 °C. The upper aqueous phase was transferred to a fresh RNase-free tube, mixed with 400 µL chloroform, vortexed and spun for 10 min at 20.000 rcf at 4 °C. The upper aqueous phase was transferred to a fresh RNase-free tube, and the RNA was precipitated by adding 55uL 3M NaOAc pH5.2 and 550 uL isopropanol, and incubated at -20 °C for at least 2 hours. To pellet the RNA, the sample was spun for 30 min at 20.000 rcf at 4 °C, the supernatant was removed and the pellet was washed with 800 µL 80% EtOH, followed by centrifugation for 10 min at 20.000 rcf at 4 °C. The EtOH was completely removed, and the RNA pellet was resuspended in nuclease-free water.

RNA seq library preparation and sequencing

For poly(A) selection, 150 ug of total RNA in 200 uL binding buffer (10 mM Tris-HCl pH 7.5, 0.5 M LiCl, 6.7 mM EDTA) was first denatured at 80°C for 2 min, and immediately incubated on ice. 150 µL of resuspended Dynabeads® Oligo(dT)$_{25}$ (Invitrogen, 61002) were first washed twice with binding buffer, then mixed with the total RNA samples, and incubated for 5 min at room temperature. The beads were then washed twice with washing buffer (10 mM Tris-HCl pH 7.5, 0.15 M LiCl, 1 mM EDTA), then resuspended in 40 µL 10 mM Tris pH 7 followed by incubation at 80°C for 2 min to elute the poly(A) RNA. The eluted poly(A) RNA was used to generate strand-specific sequencing libraries using the NEXTflex Rapid Directional Illumina RNA-Seq Library Prep Kit (BioO) according to the manufacturer's instructions. The libraries were sequenced on an NextSeq2000 sequencer. Reads were adaptor-trimmed using cutadapt and mapped using Tophat2 following rRNA read subtraction using Bowtie2, and quantified using featureCounts. The read counts per gene were normalised to the total number of reads per sample.

For RNA extracted from the nuclear sucrose gradient fraction were processed the same way with the following adjustments: 3 ng of exogenous poly(A)-containing *in vitro* transcribed RNAs ('spike-ins' (*E. coli trpS, oppF, holB, mrsP*)) were added to 50 ug of total RNA extracted from the wild type nuclear sucrose gradient fraction. To adjust for the number of harvested nuclei within a replicate, an adjusted amount of the spike-ins was added to the 50 µg of RNA extracted from each of the Nab2 mutant nuclear sucrose gradient fraction, based on the DNA content determination of the sucrose-fractionated harvested nuclei relative to the Nab2-GFP wild type. After sequencing, spike-in reads were summed per sample and normalized to the number of total reads. Sample normalization within a replicate was performed by calculating the spike-in ratios between Nab2-GFP (set to '1'), Nab2-GFP:Nab2$^{\Delta Q\text{-}\Delta RGG\text{-}SV40NLS}$-GFP and Nab2-GFP:Nab2^{F450A}-GFP using the normalized spike-in reads. Spike-in correction of the raw counts-per-million (CPM) values was then performed by multiplying the spike-in ratio value of each sample with the CPM value of each gene. To reliably detect mRNAs in all cells in the RNA FISH confirmation experiments, a cutoff of reads >500 CPM (in the Nab2-GFP average of the 3 biological replicates) was introduced. These most abundant transcripts were then further processed in the gene ontology (GO) term analysis using DAVID (Database for Annotation, Visualization and Integrated Discovery) functional annotation tool with medium stringency, 2021 update (Huang et al., 2009a, 2009b).

Protein expression and purification

All recombinantly expressed Nab2 proteins were amplified from yeast genomic DNA of the yeast strains used in this study and cloned into pETMCN-based expression vector with a cleavable N-terminal 6×His-TwinStrep tag plus a C-terminal mGFPA206K tags. Plasmids are listed in Supplementary Table 3. The plasmids were transformed into chemically competent E. coli BL21* under the selection of 0.1 mg/mL

ampicillin. Pre-cultures were grown in LB at 37 °C overnight, and diluted 1:100 into rich medium the next morning. Cells were grown at 37 °C to an OD_{600} of 0.6 and induced with final 200 mM IPTG. Cells were then grown overnight at 18 °C, collected and resuspended in 30 ml lysis buffer (500 mM NaCl, 25 mM Tris-HCl pH 7.5, 10 mM imidazole, 10% glycerol, protease inhibitors) per cell pellet from 2L of culture. After cell lysis by EmulsiFlex (Avestin), the 6×His-tagged proteins were affinity extracted with Ni^{2+} sepharose in small columns, supplemented with prescission (3C) protease for cleavage of the 6xHis-TwinStrep tag, and dialysed into storage buffer (200 mM NaCl, 25 mM Tris-HCl pH 7.5, 10 mM imidazole, 5% glycerol). The next day, protein solutions were further concentrated and purified by size exclusion with a Superdex 200 column on an AEKTA purifier (GE Life Sciences) in the final storage buffer (200 mM NaCl, 25 mM Tris-HCl pH 7.5, 10 mM imidazole, 5% glycerol). Protein expression levels, His eluates and gel filtration fractions were analysed by SDS–PAGE. Clean Superdex elution fractions were pooled, concentrated to approximately 500 μM using Millipore Amicon Centrifugation units, snap frozen as 20 μL aliquots in siliconized tubes in liquid nitrogen and stored at −80 °C. Dbp5ΔN constructs were purified according to the same protocol.

***In vitro* droplet formation assay**

A) Nab2-GFP wild type and mutant experimental setup:
   Protein droplets were set up according to (Hondele et al., 2019). In brief, reactions were pipetted in 384-well microscopy plates (Brooks, Matrical MGB101-1-2-LG-L). 2 μL recombinant GFP-tagged protein (stock 195 μM to a final concentration of 23 μM) was mixed at room temperature with 15 μL of a master mix (10.875 μL low-salt buffer (LSB; variable: LSB-100 (100 mM KCl, 30 mM HEPES-KOH pH 7.4, 2 mM $MgCl_2$) or LSB-150 (150 mM KCl, 30 mM HEPES-KOH pH 7.4, 2 mM $MgCl_2$)), 0.675 μL CKM reconstitution mix (40 mM ATP, 40 mM $MgCl_2$, 200 mM creatine phosphate, 70 U ml−1 creatine kinase), 1.35 μL ATP/MgCl2 (100 mM), 0.675 μL BSA (10 mg mL−1), 0.675 μL poly(A) RNA (1 mg mL-1), 0.675 μL 1M HEPES (variable: pH 6.6/6.8/7.0/7.2/7.4), 0.075 μL RNasin Plus (Promega). For final concentration of 11.5 μL, 1 μL Nab2-GFP (from 195 μM stock) was mixed with 16 μL of the aforementioned master mix. For final concentration of 34.5 μL, 3 μL Nab2-GFP (from 195 μM stock) was mixed with 14 μL of the aforementioned master mix.
   Droplets were imaged 20-30 min after setup at 25 °C. Microscopy was performed using an inverted epi-fluorescence microscope (Nikon Ti) equipped with a Spectra X LED light source and a Hamamatsu Flash 4.0 sCMOS camera using a 100X Plan-Apo objective NA 1.4 and NIS Elements software. Images were processed using FIJI software.
B) Nab2+Dbp5 experimental setup:
   2 μl of a 100 μM Nab2 solution was mixed with a total of 3 μl Dbp5ΔN protein (WT or mutant) mixed with Dbp5 storage buffer (200 mM NaCl, 25 mM Tris pH 7.5, 5 % glycerol) to achieve the final concentration as indicated. The final volume of 5 μl protein solution was mixed with 20 μL master mix (16 μL LSB100 buffer (100 mM KCl, 30 mM HEPES-KOH pH 7.4, 2 mM $MgCl_2$), 1 μL 10 mg/ml BSA, 1 μL 100 mM ATP / 100 mM $MgCl_2$, 1 μl HEPES-KOH pH 6.2, 1 μL poly(A) 1 mg/mL). Reactions were incubated for 10 minutes at room temperature and images recorded as described above.

Acknowledgements

We thank S. Wente and A. Corbett for providing yeast strains and plasmids, ScopeM and J. Kusch for microscopy support, L. Malinovska for experimental assistance and discussions, and the Weis lab for critical comments on the manuscript. This work was supported by an EMBO long-term fellowship to S.H. and M.H. (ALTF 290-2014, EMBOCOFUND2012, GA-2012-600394 to S.H.; ALTF 870-2014 to

M.H.). M.H. was supported by a Human Frontier Science Program (HFSP) postdoctoral fellowship (LT000914/2015) and an ETH postdoctoral fellowship (FEL-37-14-2). This work was supported by the Swiss National Science Foundation (SNF 31003A_179275 and CRSII5_193740 to K.W.).

Competing Interest Statement

The authors have declared no competing interest.

Author contributions

Conceptualization, S.H., M.H. and K.W.; Methodology, S.H., M.H., D.G. and K.W.; Investigation, S.H., M.H., C.P.D., D.M., M.Z., R.M.; Formal analysis, S.H., M.Z., A.O., F.U.; Writing – Original Draft, S.H.; Writing – Review & Editing, S.H., M.H., D.M., M.Z., R.M., A.O., F.U. and K.W.; Funding Acquisition, S.H., M.H. and K.W.; Resources, K.W.; Supervision, S.H. and K.W.

References

Adams, R.L., and Wente, S.R. (2020). Dbp5 associates with RNA-bound Mex67 and Nab2 and its localization at the nuclear pore complex is sufficient for mRNP export and cell viability. PLOS Genet. *16*, e1009033.

Aibara, S., Gordon, J.M.B., Riesterer, A.S., McLaughlin, S.H., and Stewart, M. (2017). Structural basis for the dimerization of Nab2 generated by RNA binding provides insight into its contribution to both poly(A) tail length determination and transcript compaction in Saccharomyces cerevisiae. Nucleic Acids Res. *45*, 1529–1538.

Alcázar-Román, A.R., Tran, E.J., Guo, S., and Wente, S.R. (2006). Inositol hexakisphosphate and Gle1 activate the DEAD-box protein Dbp5 for nuclear mRNA export. Nat. Cell Biol. *8*, 711–716.

Alpert, T., Straube, K., Oesterreich, F.C., and Neugebauer, K.M. (2020). Widespread Transcriptional Readthrough Caused by Nab2 Depletion Leads to Chimeric Transcripts with Retained Introns. Cell Rep. *33*, 108324.

Anderson, J.T., Wilson, S.M., Datar, K.V., and Swanson, M.S. (1993). NAB2: a yeast nuclear polyadenylated RNA-binding protein essential for cell viability. Mol. Cell. Biol. *13*, 2730–2741.

Aris, J.P., and Blobel, G. (1991). Isolation of yeast nuclei. In Methods in Enzymology. *194*, 735–749.

Ashkenazy-Titelman, A., Shav-Tal, Y., and Kehlenbach, R.H. (2020). Into the basket and beyond: the journey of mRNA through the nuclear pore complex. Biochem. J. *477*, 23–44.

Bahar Halpern, K., Caspi, I., Lemze, D., Levy, M., Landen, S., Elinav, E., Ulitsky, I., and Itzkovitz, S. (2015). Nuclear Retention of mRNA in Mammalian Tissues. Cell Rep. *13*, 2653–2662

Banani, S.F., Lee, H.O., Hyman, A.A., and Rosen, M.K. (2017). Biomolecular condensates: organizers of cellular biochemistry. Nat. Rev. Mol. Cell Biol. *18*, 285–298.

Bancaud, A., Huet, S., Rabut, G., and Ellenberg, J. (2010). Fluorescence Perturbation Techniques to Study Mobility and Molecular Dynamics of Proteins in Live Cells: FRAP, Photoactivation, Photoconversion, and FLIP. Cold Spring Harb. Protoc. *2010*, pdb.top90.

De Magistris, P. (2021). The Great Escape: mRNA Export through the Nuclear Pore Complex. Int. J. Mol. Sci. *22*, 11767.

Dechant, R., Saad, S., Ibáñez, A.J., and Peter, M. (2014). Cytosolic pH Regulates Cell Growth through Distinct GTPases, Arf1 and Gtr1, to Promote Ras/PKA and TORC1 Activity. Mol. Cell *55*, 409–421.

Derrer, C.P., Mancini, R., Vallotton, P., Huet, S., Weis, K., and Dultz, E. (2019). The RNA export factor Mex67 functions as a mobile nucleoporin. J. Cell Biol. *218* (*12*), 3967–3976

Fasken, M.B., Corbett, A.H., and Stewart, M. (2019). Structure–function relationships in the Nab2 polyadenosine-RNA binding Zn finger protein family. Protein Sci. *28*, 513–523.

Green, D.M., Johnson, C.P., Hagan, H., and Corbett, A.H. (2003). The C-terminal domain of myosin-like protein 1 (Mlp1p) is a docking site for heterogeneous nuclear ribonucleoproteins that are required for mRNA export. Proc. Natl. Acad. Sci. *100*, 1010–1015.

Hector, R.E., Nykamp, K.R., Dheur, S., Anderson, J.T., Non, P.J., Urbinati, C.R., Wilson, S.M., Minvielle-Sebastia, L., and Swanson, M.S. (2002). Dual requirement for yeast hnRNP Nab2p in mRNA poly(A) tail length control and nuclear export. EMBO J. *21*, 1800–1810.

Herzel, L., Ottoz, D.S.M., Alpert, T., and Neugebauer, K.M. (2017). Splicing and transcription touch base: co-transcriptional spliceosome assembly and function. Nat. Rev. Mol. Cell Biol. *18*, 637–650.

Hilliker, A., Gao, Z., Jankowsky, E., and Parker, R. (2011). The DEAD-Box Protein Ded1 Modulates Translation by the Formation and Resolution of an eIF4F-mRNA Complex. Mol. Cell *43*, 962–972.

Ho, B., Baryshnikova, A., and Brown, G.W. (2018). Unification of Protein Abundance Datasets Yields a Quantitative Saccharomyces cerevisiae Proteome. Cell Syst. *6*, 192-205.e3.

Hochberg-Laufer, H., Schwed-Gross, A., Neugebauer, K.M., and Shav-Tal, Y. (2019). Uncoupling of nucleo-cytoplasmic RNA export and localization during stress. Nucleic Acids Res. *47*, 4778–4797.

Hodge, C.A., Colot, H.V., Stafford, P., and Cole, C.N. (1999). Rat8p/Dbp5p is a shuttling transport factor that interacts with Rat7p/Nup159p and Gle1p and suppresses the mRNA export defect of xpo1-1 cells. EMBO J. *18*, 5778–5788.

Hondele, M., Sachdev, R., Heinrich, S., Wang, J., Vallotton, P., Fontoura, B.M.A., and Weis, K. (2019). DEAD-box ATPases are global regulators of phase-separated organelles. Nature. *573 (7772)*, 144-148

Huang, D.W., Sherman, B.T., and Lempicki, R.A. (2009a). Bioinformatics enrichment tools: paths toward the comprehensive functional analysis of large gene lists. Nucleic Acids Res. *37*, 1–13.

Huang, D.W., Sherman, B.T., and Lempicki, R.A. (2009b). Systematic and integrative analysis of large gene lists using DAVID bioinformatics resources. Nat. Protoc. *4*, 44–57.

Iserman, C., Desroches Altamirano, C., Jegers, C., Friedrich, U., Zarin, T., Fritsch, A.W., Mittasch, M., Domingues, A., Hersemann, L., Jahnel, M., et al. (2020). Condensation of Ded1p Promotes a Translational Switch from Housekeeping to Stress Protein Production. Cell *181*, 818-831.e19.

Izaurralde, E., Lewis, J., McGuigan, C., Jankowska, M., Darzynkiewicz, E., and Mattaj, I.W. (1994). A nuclear cap binding protein complex involved in pre-mRNA splicing. Cell *78*, 657–668.

Izawa, S., Takemura, R., Ikeda, K., Fukuda, K., Wakai, Y., and Inoue, Y. (2005). Characterization of Rat8 localization and mRNA export in Saccharomyces cerevisiae during the brewing of Japanese sake. Appl. Microbiol. Biotechnol. *69*, 86–91.

Joyner, R.P., Tang, J.H., Helenius, J., Dultz, E., Brune, C., Holt, L.J., Huet, S., Müller, D.J., and Weis, K. (2016). A glucose-starvation response regulates the diffusion of macromolecules. ELife *5*, e09376.

Katahira, J. (2012). mRNA export and the TREX complex. Biochim. Biophys. Acta BBA - Gene Regul. Mech. *1819*, 507–513.

Khong, A., Matheny, T., Jain, S., Mitchell, S.F., Wheeler, J.R., and Parker, R. (2017). The Stress Granule Transcriptome Reveals Principles of mRNA Accumulation in Stress Granules. Mol. Cell *68*, 808-820.e5.

Kroschwald, S., Maharana, S., Mateju, D., Malinovska, L., Nüske, E., Poser, I., Richter, D., and Alberti, S. (2015). Promiscuous interactions and protein disaggregases determine the material state of stress-inducible RNP granules. ELife *4*, e06807.

Larson, D.R., Zenklusen, D., Wu, B., Chao, J.A., and Singer, R.H. (2011). Real-Time Observation of Transcription Initiation and Elongation on an Endogenous Yeast Gene. Science *332*, 475–478.

Laughery, M.F., Hunter, T., Brown, A., Hoopes, J., Ostbye, T., Shumaker, T., and Wyrick, J.J. (2015). New vectors for simple and streamlined CRISPR-Cas9 genome editing in Saccharomyces cerevisiae. Yeast Chichester Engl. *32*, 711–720.

Li, X., Romero, P., Rani, M., Dunker, A.K., and Obradovic, Z. (1999). Predicting Protein Disorder for N-, C-, and Internal Regions. Genome Inform. Workshop Genome Inform. *10*, 30–40.

Longtine, M.S., Mckenzie III, A., Demarini, D.J., Shah, N.G., Wach, A., Brachat, A., Philippsen, P., and Pringle, J.R. (1998). Additional modules for versatile and economical PCR-based gene deletion and modification in Saccharomyces cerevisiae. Yeast *14*, 953–961.

Marfatia, K.A., Crafton, E.B., Green, D.M., and Corbett, A.H. (2003). Domain Analysis of the Saccharomyces cerevisiae Heterogeneous Nuclear Ribonucleoprotein, Nab2p dissecting the requirements for Nab2p-facilitated Poly(A) RNA export. J. Biol. Chem. *278*, 6731–6740.

Martínez-Muñoz, G.A., and Kane, P. (2008). Vacuolar and Plasma Membrane Proton Pumps Collaborate to Achieve Cytosolic pH Homeostasis in Yeast. J. Biol. Chem. *283*, 20309–20319.

Mauger, O., Lemoine, F., and Scheiffele, P. (2016). Targeted Intron Retention and Excision for Rapid Gene Regulation in Response to Neuronal Activity. Neuron *92*, 1266–1278.

Montpetit, B., Thomsen, N.D., Helmke, K.J., Seeliger, M.A., Berger, J.M., and Weis, K. (2011). A conserved mechanism of DEAD-box ATPase activation by nucleoporins and InsP6 in mRNA export. Nature *472*, 238–242.

Mugler, C.F., Hondele, M., Heinrich, S., Sachdev, R., Vallotton, P., Koek, A.Y., Chan, L.Y., and Weis, K. (2016). ATPase activity of the DEAD-box protein Dhh1 controls processing body formation. ELife *5*, e18746.

Neville, M., and Rosbash, M. (1999). The NES-Crm1p export pathway is not a major mRNA export route in Saccharomyces cerevisiae. EMBO J. *18*, 3746–3756.

Niepel, M., Farr, J.C., Rout, M.P., and Strambio-De-Castillia, C. (2017). Rapid isolation of functionally intact nuclei from the yeast Saccharomyces. BioRxiv 162388.

Nishimura, K., Fukagawa, T., Takisawa, H., Kakimoto, T., and Kanemaki, M. (2009). An auxin-based degron system for the rapid depletion of proteins in nonplant cells. Nat. Methods *6*, 917–922.

Noble, K.N., Tran, E.J., Alcázar-Román, A.R., Hodge, C.A., Cole, C.N., and Wente, S.R. (2011). The Dbp5 cycle at the nuclear pore complex during mRNA export II: nucleotide cycling and mRNP remodeling by Dbp5 are controlled by Nup159 and Gle1. Genes Dev. *25*, 1065–1077.

Orij, R., Postmus, J., Beek, A.T., Brul, S., and Smits, G.J. (2009). In vivo measurement of cytosolic and mitochondrial pH using a pH-sensitive GFP derivative in Saccharomyces cerevisiae reveals a relation between intracellular pH and growth. Microbiology *155*, 268–278.

Pühringer, T., Hohmann, U., Fin, L., Pacheco-Fiallos, B., Schellhaas, U., Brennecke, J., and Plaschka, C. (2020). Structure of the human core transcription-export complex reveals a hub for multivalent interactions. ELife *9*, e61503.

Rajoo, S., Vallotton, P., Onischenko, E., and Weis, K. (2018). Stoichiometry and compositional plasticity of the yeast nuclear pore complex revealed by quantitative fluorescence microscopy. Proc. Natl. Acad. Sci. 201719398.

Rambout, X., and Maquat, L.E. (2020). The nuclear cap-binding complex as choreographer of gene transcription and pre-mRNA processing. Genes Dev. *34*, 1113–1127.

Riback, J.A., Katanski, C.D., Kear-Scott, J.L., Pilipenko, E.V., Rojek, A.E., Sosnick, T.R., and Drummond, D.A. (2017). Stress-Triggered Phase Separation Is an Adaptive, Evolutionarily Tuned Response. Cell *168*, 1028-1040.e19.

Roden, C., and Gladfelter, A.S. (2021). RNA contributions to the form and function of biomolecular condensates. Nat. Rev. Mol. Cell Biol. *22*, 183–195.

Romero, P., Obradovic, Z., and Dunker, A.K. (1997). Sequence Data Analysis for Long Disordered Regions Prediction in the Calcineurin Family. Genome Inform. Workshop Genome Inform. *8*, 110–124.

Schmid, M., Poulsen, M.B., Olszewski, P., Pelechano, V., Saguez, C., Gupta, I., Steinmetz, L.M., Moore, C., and Jensen, T.H. (2012). Rrp6p Controls mRNA Poly(A) Tail Length and Its Decoration with Poly(A) Binding Proteins. Mol. Cell *47*, 267–280.

Schmid, M., Olszewski, P., Pelechano, V., Gupta, I., Steinmetz, L.M., and Jensen, T.H. (2015). The Nuclear PolyA-Binding Protein Nab2p Is Essential for mRNA Production. Cell Rep. *12(1),* 128-139.

Sheth, U., and Parker, R. (2003). Decapping and Decay of Messenger RNA Occur in Cytoplasmic Processing Bodies. Science *300*, 805–808.

Shi, Y., and Manley, J.L. (2015). The end of the message: multiple protein–RNA interactions define the mRNA polyadenylation site. Genes Dev. *29*, 889–897.

Shin, Y., and Brangwynne, C.P. (2017). Liquid phase condensation in cell physiology and disease. Science *357(6357),* eaaf4382.

Singh, G., Pratt, G., Yeo, G.W., and Moore, M.J. (2015). The Clothes Make the mRNA: Past and Present Trends in mRNP Fashion. Annu. Rev. Biochem. *84*, 325–354.

Smith, C., Lari, A., Derrer, C.P., Ouwehand, A., Rossouw, A., Huisman, M., Dange, T., Hopman, M., Joseph, A., Zenklusen, D., et al. (2015). In vivo single-particle imaging of nuclear mRNA export in budding yeast demonstrates an essential role for Mex67p. J. Cell Biol. *211*, 1121–1130.

Snay-Hodge, C.A., Colot, H.V., Goldstein, A.L., and Cole, C.N. (1998). Dbp5p/Rat8p is a yeast nuclear pore-associated DEAD-box protein essential for RNA export. EMBO J. *17*, 2663–2676.

Soniat, M., Sampathkumar, P., Collett, G., Gizzi, A.S., Banu, R.N., Bhosle, R.C., Chamala, S., Chowdhury, S., Fiser, A., Glenn, A.S., et al. (2013). Crystal structure of human Karyopherin β2 bound to the PY-NLS of Saccharomyces cerevisiae Nab2. J. Struct. Funct. Genomics *14*, 31–35.

Soucek, S., Zeng, Y., Bellur, D.L., Bergkessel, M., Morris, K.J., Deng, Q., Duong, D., Seyfried, N.T., Guthrie, C., Staley, J.P., et al. (2016). Evolutionarily Conserved Polyadenosine RNA Binding Protein Nab2 Cooperates with Splicing Machinery To Regulate the Fate of Pre-mRNA. Mol. Cell. Biol. *36*, 2697–2714.

Sträßer, K., and Hurt, E. (2001). Splicing factor Sub2p is required for nuclear mRNA export through its interaction with Yra1p. Nature *413*, 648–652.

Strässer, K., Masuda, S., Mason, P., Pfannstiel, J., Oppizzi, M., Rodriguez-Navarro, S., Rondón, A.G., Aguilera, A., Struhl, K., Reed, R., et al. (2002). TREX is a conserved complex coupling transcription with messenger RNA export. Nature *417*, 304–308.

Takemura, R., Inoue, Y., and Izawa, S. (2004). Stress response in yeast mRNA export factor: reversible changes in Rat8p localization are caused by ethanol stress but not heat shock. J. Cell Sci. *117*, 4189–4197.

Tauber, D., Tauber, G., Khong, A., Treeck, B.V., Pelletier, J., and Parker, R. (2020). Modulation of RNA Condensation by the DEAD-Box Protein eIF4A. Cell *180(3),* 411-426.

Teixeira, D., and Parker, R. (2007). Analysis of P-Body Assembly in Saccharomyces cerevisiae. Mol. Biol. Cell *18*, 2274–2287.

Tipper, D.J. (1973). Inhibition of Yeast Ribonucleic Acid Polymerases by Thiolutin. J. Bacteriol. *116(1)*, 245-56

Tran, E.J., Zhou, Y., Corbett, A.H., and Wente, S.R. (2007). The DEAD-Box Protein Dbp5 Controls mRNA Export by Triggering Specific RNA:Protein Remodeling Events. Mol. Cell *28*, 850–859.

Tuck, A.C., and Tollervey, D. (2013). A Transcriptome-wide Atlas of RNP Composition Reveals Diverse Classes of mRNAs and lncRNAs. Cell *154*, 996–1009.

Vallotton, P., Rajoo, S., Wojtynek, M., Onischenko, E., Kralt, A., Derrer, C.P., and Weis, K. (2019). Mapping the native organization of the yeast nuclear pore complex using nuclear radial intensity measurements. Proc. Natl. Acad. Sci. *116*, 14606–14613.

Wegener, M., and Müller-McNicoll, M. (2019). View from an mRNP: The Roles of SR Proteins in Assembly, Maturation and Turnover. In: Oeffinger M., Zenklusen D. (eds) The Biology of mRNA: Structure and Function. Advances in Experimental Medicine and Biology, vol 1203. Springer, Cham. https://doi.org/10.1007/978-3-030-31434-7_3.

Weirich, C.S., Erzberger, J.P., Flick, J.S., Berger, J.M., Thorner, J., and Weis, K. (2006). Activation of the DExD/H-box protein Dbp5 by the nuclear-pore protein Gle1 and its coactivator InsP6 is required for mRNA export. Nat. Cell Biol. *8*, 668–676.

Yang, P., Mathieu, C., Kolaitis, R.-M., Zhang, P., Messing, J., Yurtsever, U., Yang, Z., Wu, J., Li, Y., Pan, Q., et al. (2020). G3BP1 Is a Tunable Switch that Triggers Phase Separation to Assemble Stress Granules. Cell *181*, 325-345.e28.

Figure legends

1) **Acute Dbp5 depletion causes nuclear mRNA accumulation and Nab2 condensation**
   A) Schematic representation of the auxin-inducible protein depletion tool and the single RNA visualization in vivo. (upper) Upon addition of Auxin, degron-tagged Dbp5 gets recognized by TIR1 and targeted for proteasomal degradation (Nishimura et al., 2009). (lower) 24 PP7 stem loops (PP7sl) are integrated after the STOP codon of a low-copy number gene of interest. A second locus drives the expression of GFP-tagged PP7 coat protein (PP7CP-GFP) that can bind to PP7sl with high affinity, thereby allowing single RNA visualization (Larson et al., 2011).
   B) Cells expressing GFA1-PP7sl, PP7CP-GFP, the nuclear rim marker Ndc1and the Dbp5-degron with or without TIR1 are treated for 1 hr with auxin (IAA) before imaging using a custom-built microscope (Smith et al., 2015). Scale bar 5 μm.
   C) Quantification of mean squared displacement (MSD) of PP7-labeled GFA1 mRNA in cells from B). Images were taken every 15 ms. Shown are means ± SD of three biological replicates with ≥265 RNA particles per condition.
   D) FRAP of Nab2-GFP cells expressing the Dbp5-degron with or without TIR1 treated for 2 hr with auxin (IAA). FRAP curves are normalized to prebleach and postbleach values. Mean curves ± SEM of three biological replicates with ≥16 cells per replicate are shown.
   E) Half time of recovery retrieved from fitting individual FRAP curves from D) with a single component model. Shown are means ± SEM of three biological replicates. * p=0.028, unpaired t-test.
   F) Representative FRAP images of a single nucleus from D)
   G) FRAP of Nab2-GFP cells expressing either only the Dbp5-degron or both the Dbp5-degron and the Rpb2-degron with or without TIR1 treated for 2 hr with auxin (IAA). FRAP curves are normalized to prebleach and postbleach values. Mean curves ± SEM of three biological replicates with ≥15 cells per replicate are shown.
   H) Half time of recovery retrieved from fitting individual FRAP curves from G) with a single component model. Shown are means ± SEM of three biological replicates. * p=0.0271 (–TIR1(+Dbp5) vs. +TIR1(–Dbp5), * p=0.0232 +TIR1(–Dbp5) vs. +TIR1(–Dbp5, –Rbp2), ns p=0.6109 ((–TIR1(+Dbp5) vs. +TIR1(–Dbp5, –Rbp2)), unpaired t-test.

2) **Nab2 phase-separates *in vitro*, which gets reverted by active Dbp5**
   A) Recombinant Nab2-GFP droplets were formed in LSB150 buffer to a final KCl concentration of 94 mM in the presence or absence of 0.04 mg/mL poly(A) RNA and imaged at 25 °C 30 min after setup. Scale bar 10 μm.
   B) Recombinant Nab2-GFP droplets were formed in LSB100 or LSB150 buffers to a final KCl concentration of 63 or 94 mM, respectively, at the indicated pH in the presence of 0.04 mg/mL poly(A) RNA and imaged at 25 °C 30 min after setup. Scale bar 10 μm.
   C) Representative images and phase diagram of recombinant Nab2-GFP droplets, which were formed in LSB150 buffer (to a final KCl concentration of 94 mM) containing the indicated single-nucleoside polymers and imaged at 25 °C 20 min after setup. Scale bar 5 μm.
   D) Recombinant Nab2-GFP droplets were formed without Dbp5 or in the presence of increasing amounts of Dbp5ΔN90 or the ATPase-locked Dbp5-ΔN90-DQAD and imaged at 25 °C 30 min after setup. Nab2 9 μM in LSB100 (final 63 mM KCl), 0.04 mg/mL poly(A) RNA, Dbp5 concentrations 14/27/39 μM. Scale bar 10 μm.

3) **Glucose stress causes reduction of nuclear Nab2 dynamics and bulk nuclear RNA retention**
   A) Cells expressing Dbp5-GFP and dsRed-HDEL were grown in medium + DEX or acutely shifted for 30 min or 24 hrs into medium without DEX. Scale bar 5 μm.
   B) Quantification of Dbp5-GFP intensity at the nuclear envelope by NuRIM in the conditions shown in A). Shown are means ± SEM of three biological replicates. At least 350 cells were analyzed per condition and replicate. Dbp5: ** p=0.0082 (+DEX vs. 30 min –DEX), * p=0.022 (+DEX vs. 24 hrs –DEX), unpaired t-test.
   C) RNA FISH against poly(A) using an oligo(dT)30 probe was performed in fixed cells expressing Nab2-GFP. Samples were taken in +DEX or after acute starvation in medium without DEX for 30 min. Insets show single nucleus (2.16x magnification). White arrows indicate Nab2-GFP focus. Scale bar 5 μm.
   D) RNA FISH against poly(A) RNA using an oligo(dT)30 probe was performed in fixed cells expressing Nab2-GFP. Samples were taken in +DEX or after acute starvation in medium without DEX for 24 hrs. Insets show single nucleus (2.16x magnification). White arrows indicate Nab2-GFP focus. Scale bar 5 μm.
   E) FRAP of Nab2-GFP cells in +DEX or 30 min –DEX. FRAP curves are normalized to prebleach and postbleach values. Mean curves ± SEM of three biological replicates with ≥15 cells per replicate are shown.
   F) Half time of recovery retrieved from fitting individual FRAP curves from E) with a single component model. Shown are means ± SEM of three biological replicates. * p=0.04, unpaired t-test.
   G) FRAP of Nab2-GFP cells in +DEX or 24 hrs –DEX. FRAP curves are normalized to prebleach and postbleach values. Mean curves ± SEM of three biological replicates with ≥15 cells per replicate are shown.
   H) Half time of recovery retrieved from fitting individual FRAP curves from G) with a single component model. Shown are means ± SEM of three biological replicates. * p=0.01, unpaired t-test.
   I) Representative images of Nab2-GFP cells in wild type (WT) or Dbp5-$^{\Delta N}$Nup159 ('Dbp5 tether') background in +DEX or 24 hrs –DEX. Scale bar 5 μm.
   J) FRAP of cells in I). FRAP curves are normalized to prebleach and postbleach values. Mean curves ± SEM of three biological replicates with ≥15 cells per replicate are shown.
   K) Half time of recovery retrieved from fitting individual FRAP curves from J) with a single component model. Shown are means ± SEM of three biological replicates. ns p=0.4425, * p=0.0425, ** p=0.0067 (wild type 24 hrs –DEX vs. Dbp5-$^{\Delta N}$Nup159 +DEX), ** p=0.0032 (Dbp5-$^{\Delta N}$Nup159 +DEX vs. 24 hrs –DEX), unpaired t-test.

4) **Nab2 dimerization, but not RGG domain function, drives condensation *in vitro***
   A) GFP-tagged recombinant Nab2 wild type or Nab2 mutant droplets were formed in LSB150 buffer to a final KCl concentration of 94 mM at the indicated pH in the presence of 0.04 mg/mL polyA RNA and imaged at 25 °C 30 min after setup. Right side: phase diagram of droplet formation at pH 6.8 with the indicated protein and RNA concentrations. Scale bar 10 μm.
   B) FRAP of 20 μM Nab2-GFP and Nab2$^{\Delta Q\text{-}\Delta RGG\text{-}SV40NLS}$-GFP droplets 30 min after setup with 0.04 mg/mL polyA RNA. FRAP curves are normalized to prebleach and postbleach values. Mean curves ± SEM of three biological replicates with ≥14 droplets per replicate are shown.
   C) Representative images of GFP-tagged Nab2 wild type and mutant cells in +DEX conditions and after acute shift and incubation for 24 hrs in –DEX. Scale bar 5 μm.

D-F) FRAP of cells shown in C). D) Nab2-GFP, E) Nab2$^{\Delta Q\text{-}\Delta RGG\text{-}SV40NLS}$-GFP, F) Nab2^{F450A}-GFP. FRAP curves are normalized to prebleach and postbleach values. Mean curves ± SEM of three biological replicates with ≥15 cells per replicate are shown.

G) Half time of recovery retrieved from fitting individual FRAP curves from D-F) with a single component model. Shown are means ± SEM of three biological replicates. * p=0.0155, ** p=0.0082, ns p=0.3694, unpaired t-test.

5) The degree of Nab2 condensation determines the level of nuclear mRNA retention

A) RNA FISH against poly(A) RNA using an oligo(dT)30 probe was performed in fixed cells expressing Nab2-GFP, Nab2$^{\Delta Q\text{-}\Delta RGG\text{-}SV40NLS}$-GFP or Nab2^{F450A}-GFP. Samples were taken in +DEX or after acute starvation in medium without DEX for 24 hrs. Insets show single nucleus (2.16x magnification). Scale bar 5 μm.

B) Quantification of nuclear poly(A) RNA signal intensity in 24 hrs –DEX condition in A). Data is normalized to Nab2-GFP. Shown are means ± SEM of five biological replicates, n>100 cells per replicate. ** p=0.003 (Nab2-GFP vs. Nab2$^{\Delta Q\text{-}\Delta RGG\text{-}SV40NLS}$-GFP), ** p=0.0023 (Nab2-GFP vs. Nab2^{F450A}-GFP), ** p=0.0011 (Nab2$^{\Delta Q\text{-}\Delta RGG\text{-}SV40NLS}$-GFP vs. Nab2^{F450A}-GFP), unpaired t-test.

C) Plot of ratios of nuclear RNA sequencing reads (CPM, counts per million). Single dots represent individual genes. Inset shows most abundant reads (blue dots, >500 CPM in Nab2-GFP average of 3 biological replicates, representing 42% of the total reads). Boxes highlight differentially enriched genes (Nab2$^{\Delta Q\text{-}\Delta RGG\text{-}SV40NLS}$-GFP : Nab2-GFP; purple, fold change ratio >1.5) and not differentially enriched genes (Nab2$^{\Delta Q\text{-}\Delta RGG\text{-}SV40NLS}$-GFP : Nab2-GFP; grey, fold change ratio between 0.8 and 1.2).

D) Gene ontology (GO) term analysis of most abundant reads (blue dots) from C) using DAVID Functional Annotation Clustering tool (Huang et al., 2009a, 2009b).

6) Nab2 condensation confers selective mRNA retention *in vivo* during stress

A) RNA FISH against *BTN2* was performed in fixed cells expressing Nab2-GFP, Nab2$^{\Delta Q\text{-}\Delta RGG\text{-}SV40NLS}$-GFP or Nab2^{F450A}-GFP. Samples were harvested in +DEX or after acute starvation in medium without DEX for 24 hrs. Scale bar 5 μm.

B) Quantification of 24 hrs –DEX condition in A). Shown are means ± SEM of five biological replicates, n>100 cells per replicate. ** p=0.0018 (Nab2-GFP vs. Nab2$^{\Delta Q\text{-}\Delta RGG\text{-}SV40NLS}$-GFP), ns p=0.2943 (Nab2-GFP vs. Nab2^{F450A}-GFP), ** p=0.0064 (Nab2$^{\Delta Q\text{-}\Delta RGG\text{-}SV40NLS}$-GFP vs. Nab2^{F450A}-GFP), unpaired t-test.

C) RNA FISH against *HSP42* was performed in fixed cells expressing Nab2-GFP, Nab2$^{\Delta Q\text{-}\Delta RGG\text{-}SV40NLS}$-GFP or Nab2^{F450A}-GFP. Samples were harvested in +DEX or after acute starvation in medium without DEX for 24 hrs. Scale bar 5 μm.

D) Quantification of 24 hrs –DEX condition in C). Data is normalized to Nab2-GFP. Shown are means ± SEM of three biological replicates, n>100 cells per replicate. * p=0.0249 (Nab2-GFP vs. Nab2$^{\Delta Q\text{-}\Delta RGG\text{-}SV40NLS}$-GFP), ns p=0.4480 (Nab2-GFP vs. Nab2^{F450A}-GFP), * p=0.0342 (Nab2$^{\Delta Q\text{-}\Delta RGG\text{-}SV40NLS}$-GFP vs. Nab2^{F450A}-GFP), unpaired t-test.

E) RNA FISH against *HXT6* was performed in fixed cells expressing Nab2-GFP, Nab2$^{\Delta Q\text{-}\Delta RGG\text{-}SV40NLS}$-GFP or Nab2^{F450A}-GFP. Samples were harvested in +DEX or after acute starvation in medium without DEX for 24 hrs. Scale bar 5 μm.

F) Quantification of 24 hrs –DEX condition in E). Data is normalized to Nab2-GFP. Shown are means ± SEM of five biological replicates, n>100 cells per replicate. ** p=0.0081 (Nab2-GFP

vs. Nab2$^{\Delta Q\text{-}\Delta RGG\text{-}SV40NLS}$-GFP), ns p=0.2777 (Nab2-GFP vs. Nab2^{F450A}-GFP), * p=0.0135 (Nab2$^{\Delta Q\text{-}\Delta RGG\text{-}SV40NLS}$-GFP vs. Nab2^{F450A}-GFP), unpaired t-test.

G) RNA FISH against *DED1* was performed in fixed cells expressing Nab2-GFP, Nab2$^{\Delta Q\text{-}\Delta RGG\text{-}SV40NLS}$-GFP or Nab2^{F450A}-GFP. Samples were harvested in +DEX or after acute starvation in medium without DEX for 24 hrs. Scale bar 5 μm.

H) Quantification of 24 hrs –DEX condition in G). Data is normalized to Nab2-GFP. Shown are means ± SEM of three biological replicates, n>100 cells per replicate. ns p=0.8324 (Nab2-GFP vs. Nab2$^{\Delta Q\text{-}\Delta RGG\text{-}SV40NLS}$-GFP), ns p=0.5458 (Nab2-GFP vs. Nab2^{F450A}-GFP), ns p=0.9009 (Nab2$^{\Delta Q\text{-}\Delta RGG\text{-}SV40NLS}$-GFP vs. Nab2^{F450A}-GFP), unpaired t-test.

7) Correct Nab2 condensation is essential for survival after prolonged stress

A) Growth recovery assay of cells expressing Nab2-GFP, Nab2$^{\Delta Q\text{-}\Delta RGG\text{-}SV40NLS}$-GFP or Nab2^{F450A}-GFP. Mid-log cultures grown in +DEX or acutely starved in medium without DEX for 24 hrs or 120 hrs were recovered as 1:5 serial dilutions (starting OD_{600} 0.2) on rich medium plates containing glucose at either 25 °C for 2 days or 37 °C for 1 day.

B) Model depicting how nuclear Nab2 condensation blocks export of bulk mRNA and allows selective transport of stress-induced mRNAs.

Figure 1

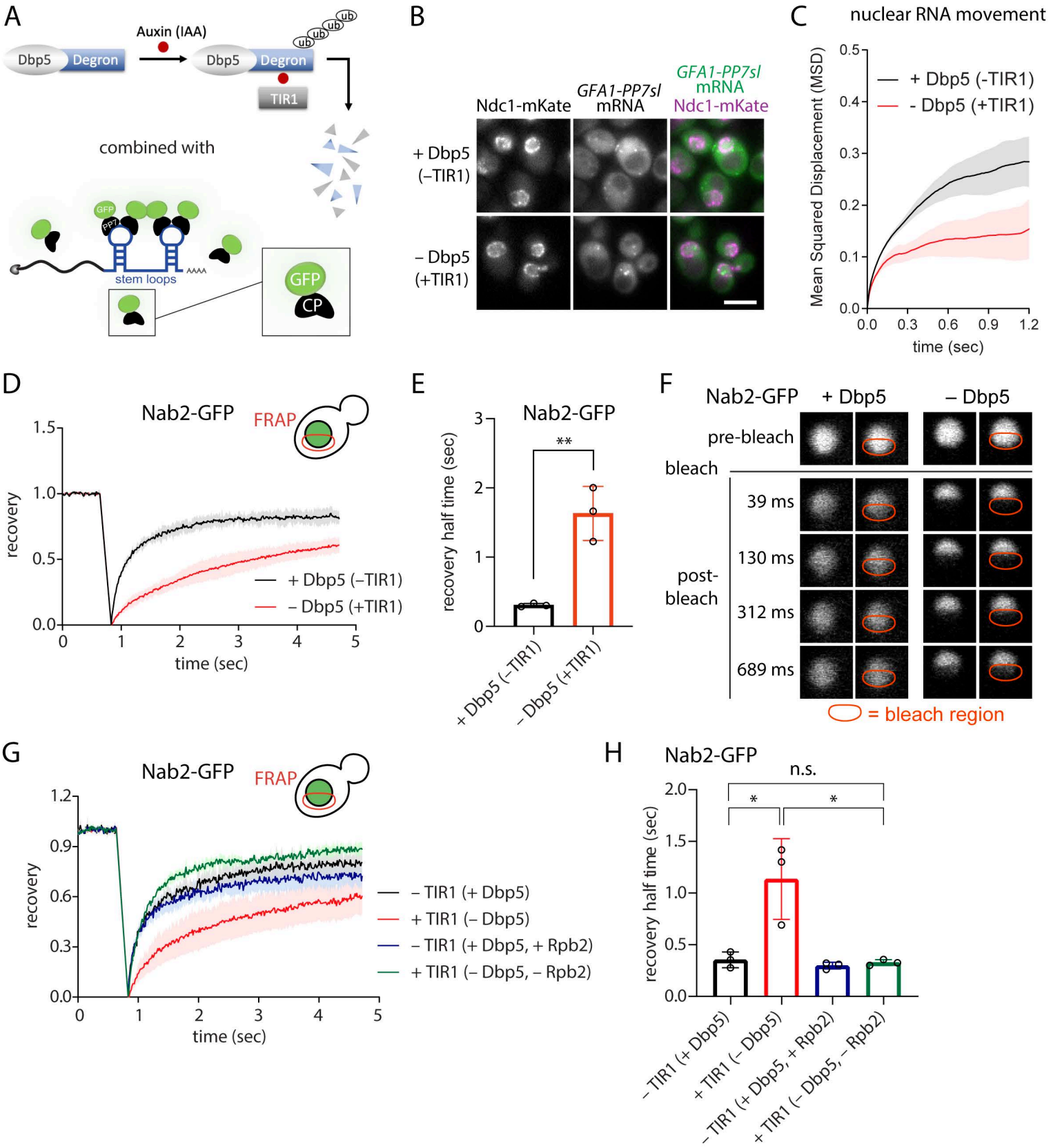
A
Auxin (IAA)
Dbp5
Degron
Dbp5
Degron
ub
TIR1
combined with
GFP
PP7
stem loops
AAAA
GFP
CP
B
Ndc1-mKate
GFA1-PP7sl mRNA
GFA1-PP7sl mRNA
Ndc1-mKate
+ Dbp5 (–TIR1)
– Dbp5 (+TIR1)
C
nuclear RNA movement
Mean Squared Displacement (MSD)
+ Dbp5 (-TIR1)
- Dbp5 (+TIR1)
time (sec)
D
Nab2-GFP
FRAP
recovery
+ Dbp5 (–TIR1)
– Dbp5 (+TIR1)
time (sec)
E
Nab2-GFP
recovery half time (sec)
**
+ Dbp5 (–TIR1)
– Dbp5 (+TIR1)
F
Nab2-GFP
+ Dbp5
– Dbp5
pre-bleach
bleach
post-bleach
39 ms
130 ms
312 ms
689 ms
= bleach region
G
Nab2-GFP
FRAP
recovery
– TIR1 (+ Dbp5)
+ TIR1 (– Dbp5)
– TIR1 (+ Dbp5, + Rpb2)
+ TIR1 (– Dbp5, – Rpb2)
time (sec)
H
Nab2-GFP
n.s.
*
*
recovery half time (sec)
– TIR1 (+ Dbp5)
+ TIR1 (– Dbp5)
– TIR1 (+ Dbp5, + Rpb2)
+ TIR1 (– Dbp5, – Rpb2)

Figure 2

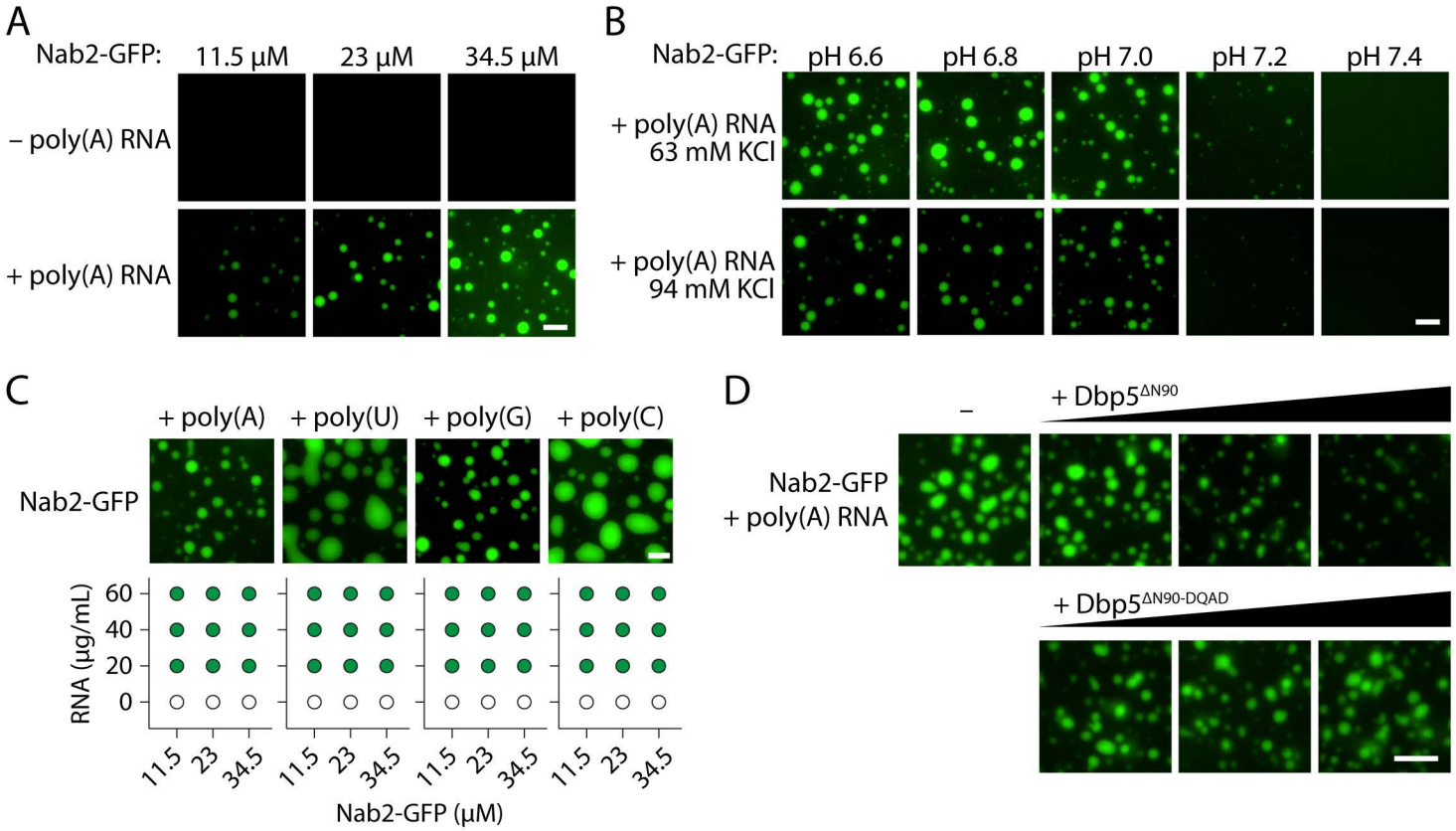
A
Nab2-GFP:
11.5 μM
23 μM
34.5 μM
– poly(A) RNA
+ poly(A) RNA
B
Nab2-GFP:
pH 6.6
pH 6.8
pH 7.0
pH 7.2
pH 7.4
+ poly(A) RNA
63 mM KCl
+ poly(A) RNA
94 mM KCl
C
+ poly(A)
+ poly(U)
+ poly(G)
+ poly(C)
Nab2-GFP
RNA (μg/mL)
60
40
20
0
11.5
23
34.5
Nab2-GFP (μM)
D
–
+ Dbp5ΔN90
Nab2-GFP
+ poly(A) RNA
+ Dbp5ΔN90-DQAD

Figure 3

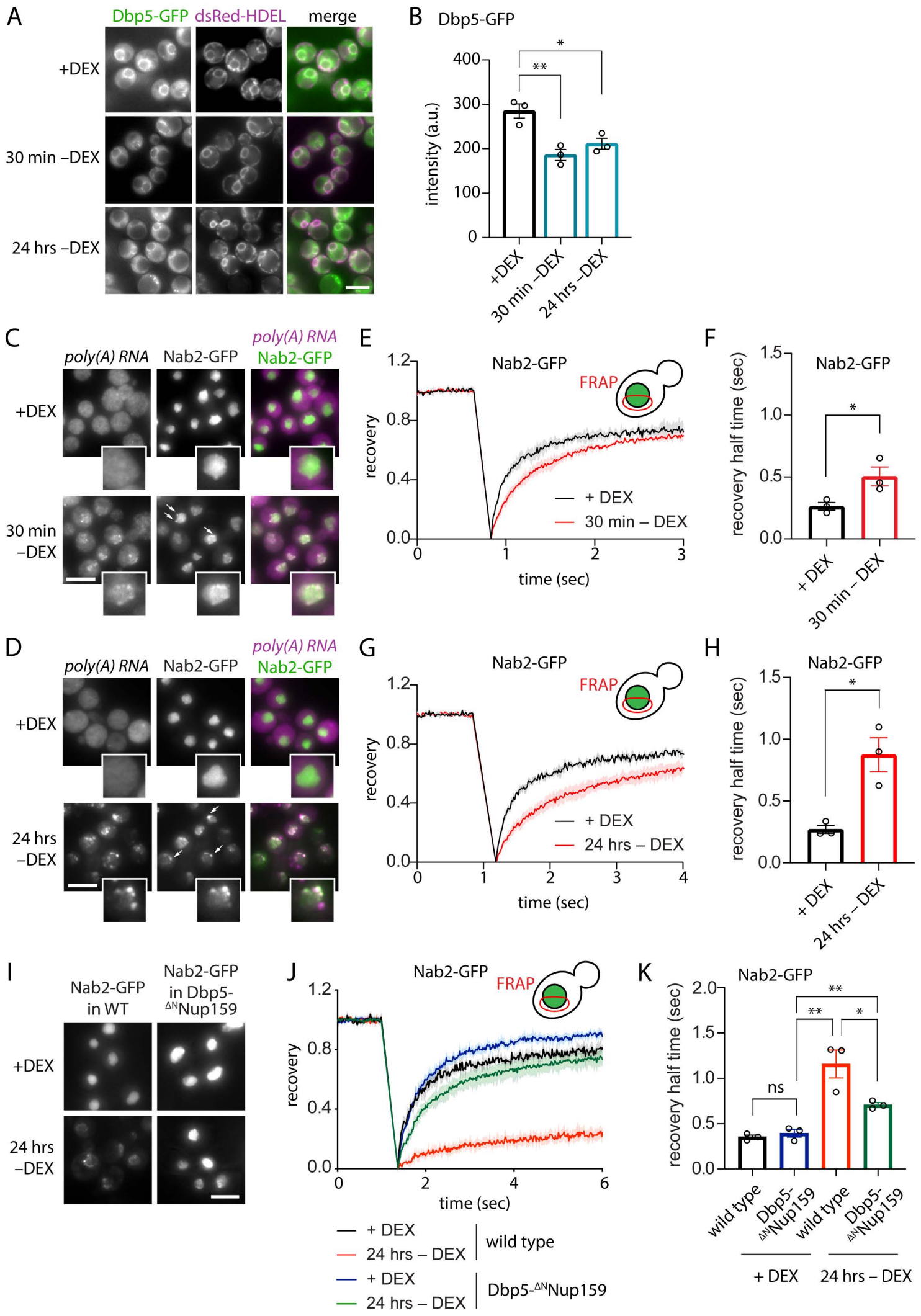
A
Dbp5-GFP
dsRed-HDEL
merge
+DEX
30 min –DEX
24 hrs –DEX
B
Dbp5-GFP
intensity (a.u.)
400
300
200
100
0
*
**
+DEX
30 min –DEX
24 hrs –DEX
C
poly(A) RNA
Nab2-GFP
poly(A) RNA
Nab2-GFP
+DEX
30 min –DEX
D
poly(A) RNA
Nab2-GFP
poly(A) RNA
Nab2-GFP
+DEX
24 hrs –DEX
E
Nab2-GFP
FRAP
recovery
1.2
0.8
0.4
0.0
0
1
2
3
time (sec)
+ DEX
30 min – DEX
F
Nab2-GFP
recovery half time (sec)
1.5
1.0
0.5
0.0
*
+ DEX
30 min – DEX
G
Nab2-GFP
FRAP
recovery
1.2
0.8
0.4
0.0
0
1
2
3
4
time (sec)
+ DEX
24 hrs – DEX
H
Nab2-GFP
recovery half time (sec)
1.5
1.0
0.5
0.0
*
+ DEX
24 hrs – DEX
I
Nab2-GFP in WT
Nab2-GFP in Dbp5-ΔNNup159
+DEX
24 hrs –DEX
J
Nab2-GFP
FRAP
recovery
1.2
0.8
0.4
0.0
0
2
4
6
time (sec)
+ DEX
24 hrs – DEX
wild type
+ DEX
24 hrs – DEX
Dbp5-ΔNNup159
K
Nab2-GFP
recovery half time (sec)
2.0
1.5
1.0
0.5
0.0
ns
**
**
*
wild type
Dbp5-ΔNNup159
wild type
Dbp5-ΔNNup159
+ DEX
24 hrs – DEX

Figure 4

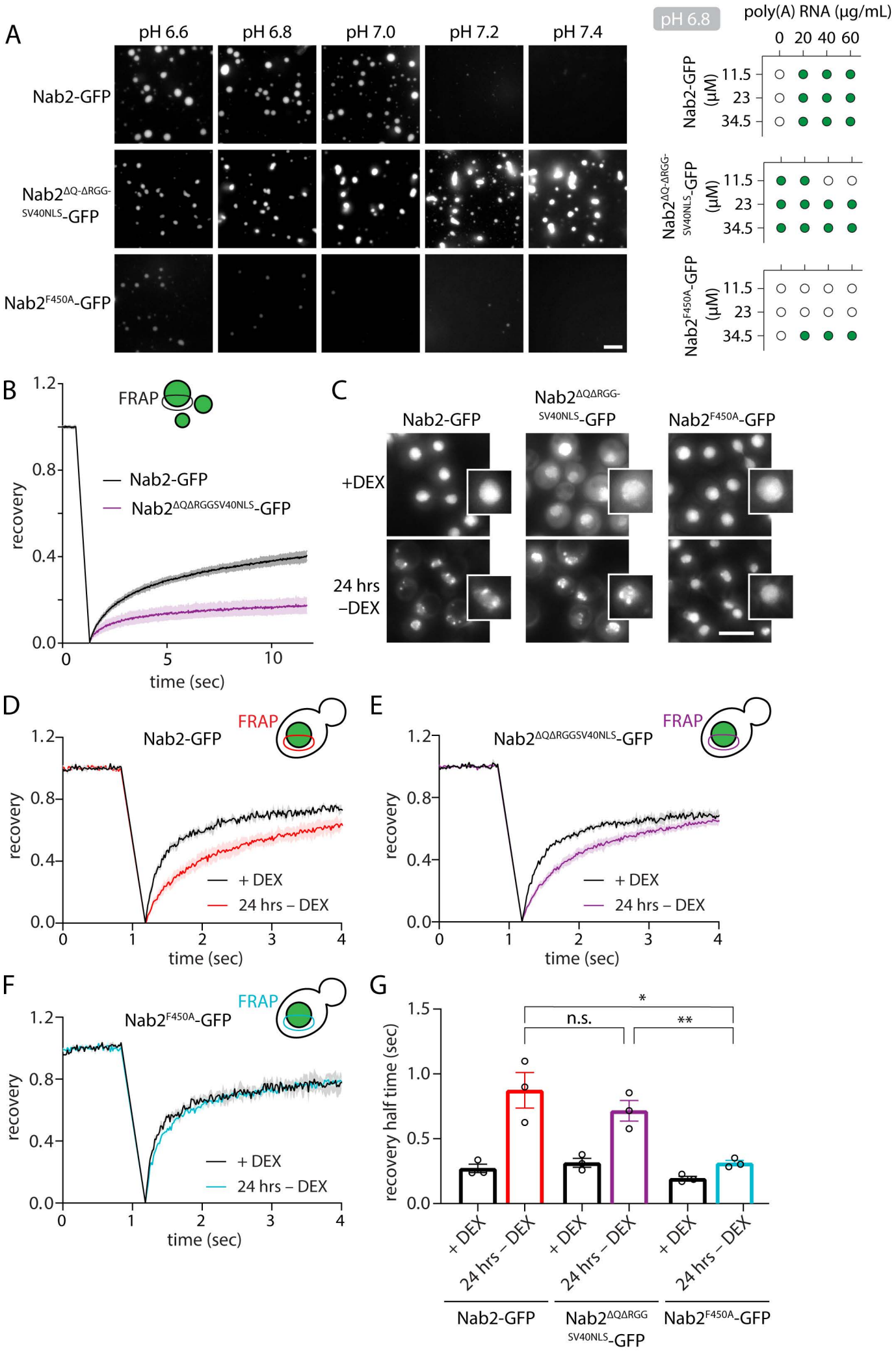
A
pH 6.6
pH 6.8
pH 7.0
pH 7.2
pH 7.4
Nab2-GFP
Nab2ΔQ-ΔRGG-SV40NLS-GFP
Nab2F450A-GFP
pH 6.8
poly(A) RNA (μg/mL)
0 20 40 60
11.5
23
34.5
(μM)
B
FRAP
recovery
time (sec)
Nab2-GFP
Nab2ΔQΔRGGSV40NLS-GFP
C
Nab2-GFP
Nab2ΔQΔRGG-SV40NLS-GFP
Nab2F450A-GFP
+DEX
24 hrs –DEX
D
Nab2-GFP
FRAP
+ DEX
24 hrs – DEX
E
Nab2ΔQΔRGGSV40NLS-GFP
FRAP
F
Nab2F450A-GFP
FRAP
G
recovery half time (sec)
n.s.
*
**
+ DEX
24 hrs – DEX
Nab2-GFP
Nab2ΔQΔRGG SV40NLS-GFP
Nab2F450A-GFP

Figure 5

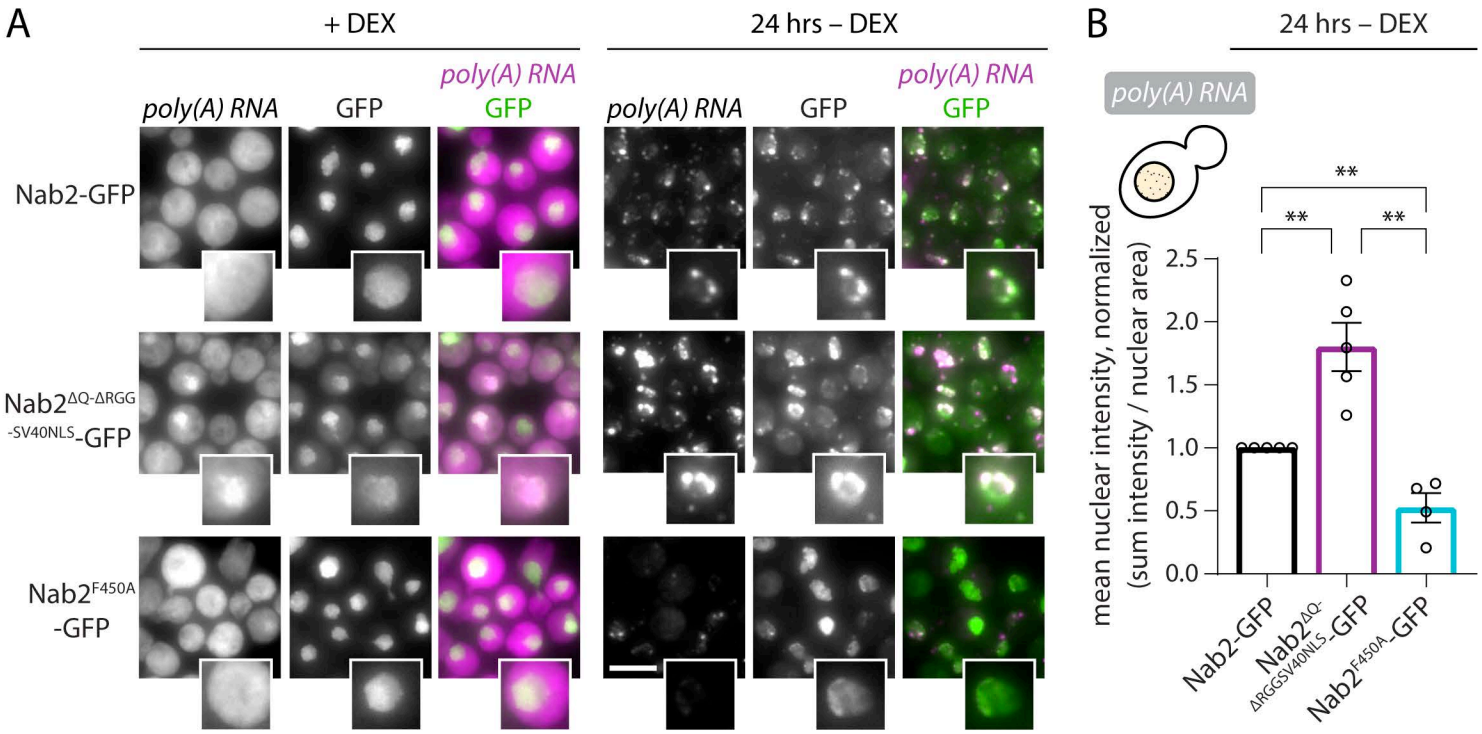

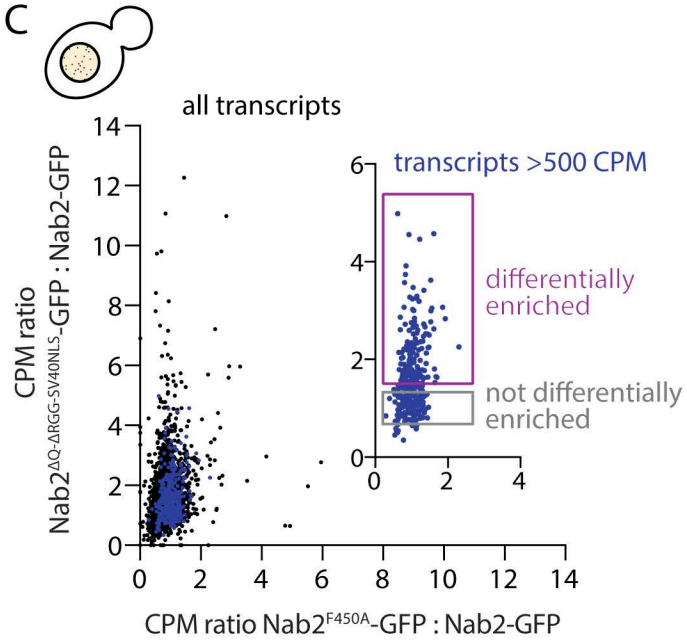

D

Nab2ΔQ-ΔRGG-SV40NLS-GFP vs. Nab2-GFP

	GO Term	# of prot.	p value
differentially enriched	protein folding	17	5.28E-10
	cellular response to oxidative stress	14	2.08E-07
	carbohydrate metabolic process	12	5.42E-05
	cellular response to heat	12	1.51E-11
	cellular oxidant detoxification	8	1.28E-06
not differentially enriched	translation	15	7.56E-06
	translation termination	10	1.02E-04
	glycolytic process	7	6.35E-07
	rRNA binding	6	5.23E-04
	gluconeogenesis	5	2.92E-05

Figure 6

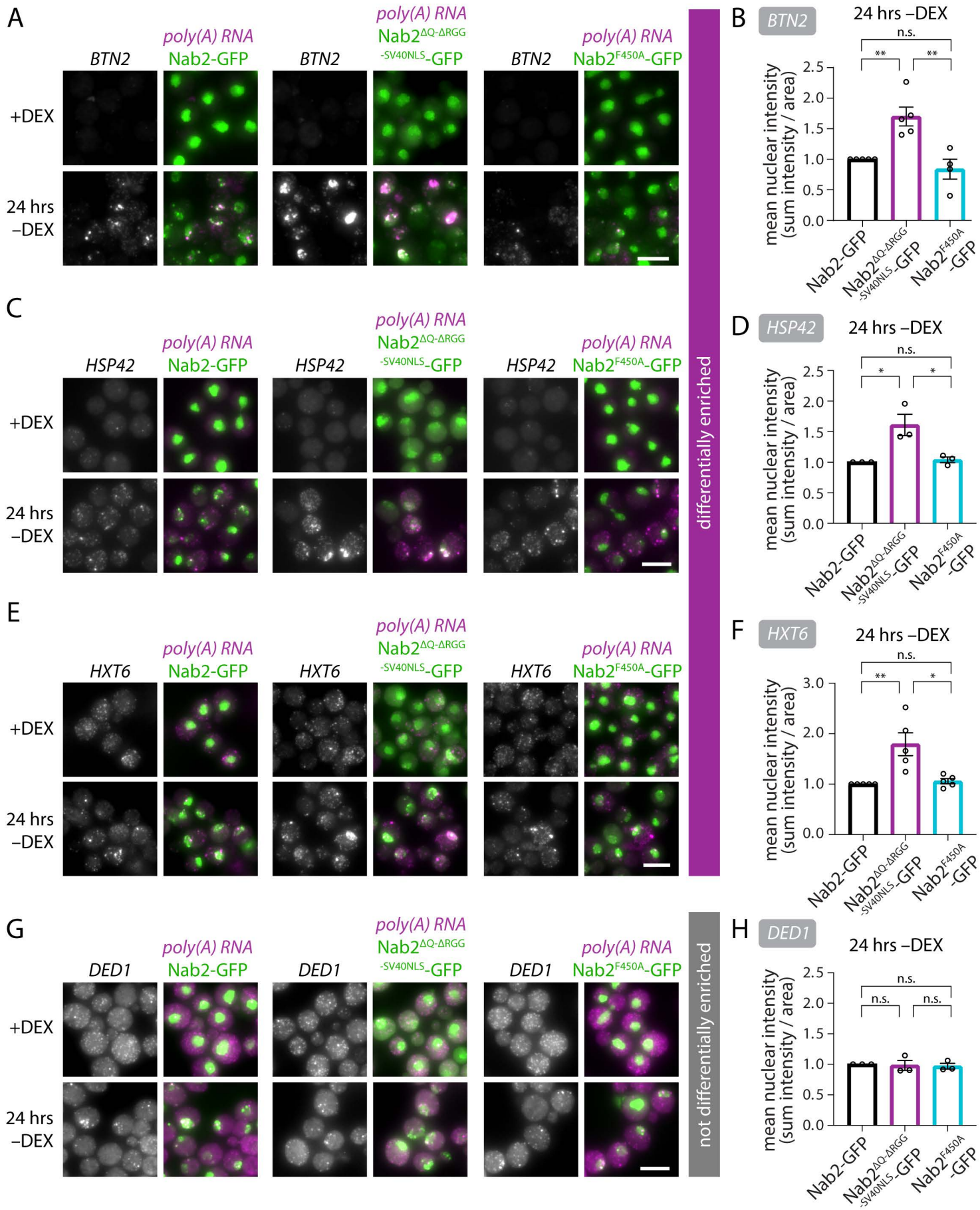
A
BTN2
poly(A) RNA Nab2-GFP
poly(A) RNA Nab2ΔQ-ΔRGG -SV40NLS-GFP
poly(A) RNA Nab2F450A-GFP
+DEX
24 hrs –DEX
B
BTN2
24 hrs –DEX
mean nuclear intensity (sum intensity / area)
n.s.
**
**
Nab2-GFP
Nab2ΔQ-ΔRGG -SV40NLS-GFP
Nab2F450A -GFP
C
HSP42
D
HSP42
*
*
E
HXT6
F
HXT6
G
DED1
H
DED1
differentially enriched
not differentially enriched

Figure 7

A

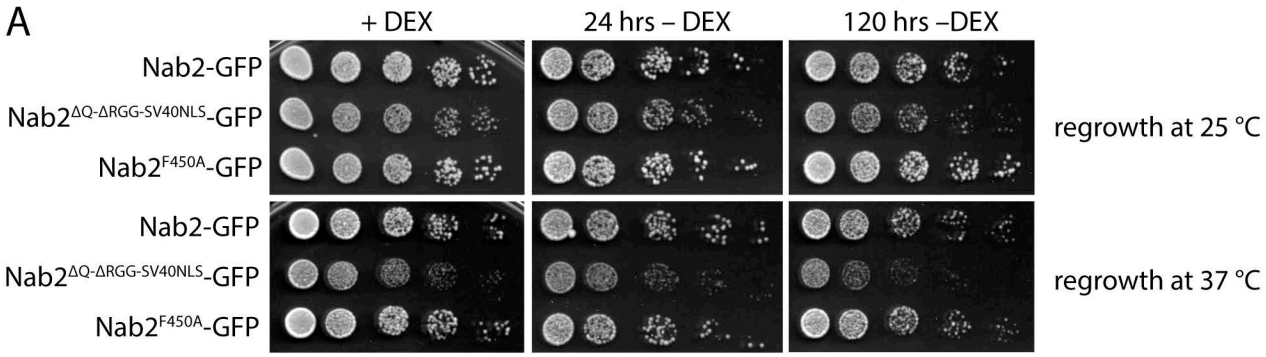
+ DEX
24 hrs – DEX
120 hrs –DEX
Nab2-GFP
Nab2ΔQ-ΔRGG-SV40NLS-GFP
Nab2F450A-GFP
regrowth at 25 °C
Nab2-GFP
Nab2ΔQ-ΔRGG-SV40NLS-GFP
Nab2F450A-GFP
regrowth at 37 °C

B

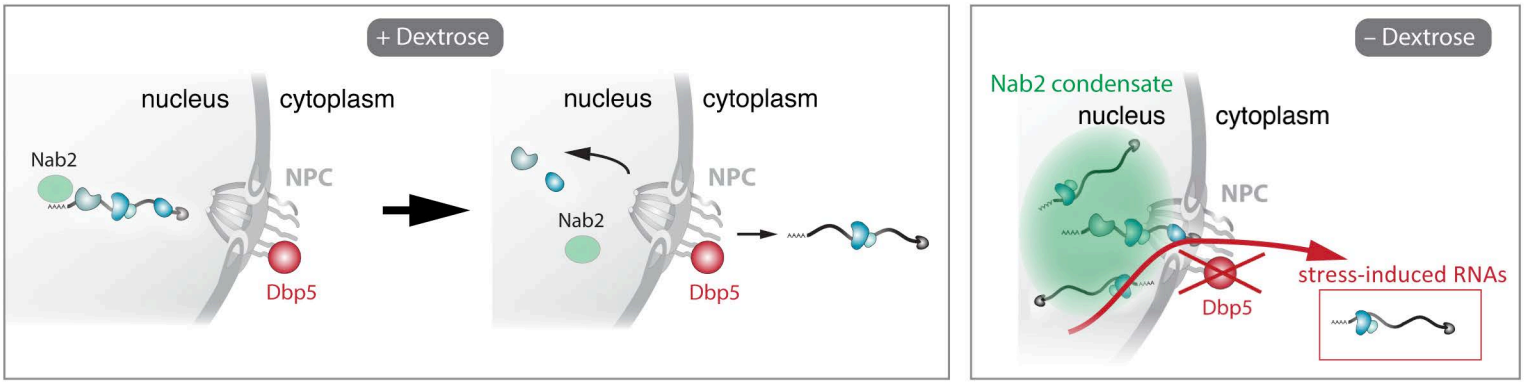
+ Dextrose
nucleus
cytoplasm
Nab2
NPC
Dbp5
nucleus
cytoplasm
Nab2
NPC
Dbp5
– Dextrose
Nab2 condensate
nucleus
cytoplasm
NPC
Dbp5
stress-induced RNAs